

1 **Field-scale CH₄ emission at a sub-arctic mire with heterogeneous permafrost thaw status**

2 Patryk Łakomic¹, Jutta Holst¹, Thomas Friborg², Patrick Crill³, Niklas Rakos⁴, Natascha Kljun⁵, Per-
3 Ola Olsson¹, Lars Eklundh¹, Andreas Persson¹, Janne Rinne¹

4 ¹ Department of Physical Geography and Ecosystem Science, Lund University, 223 62, Sweden

5 ² Department of Geosciences and Natural Resource Management, University of Copenhagen,
6 1165, Denmark

7 ³ Department of Geological Sciences and Bolin Centre for Climate Research, Stockholm
8 University, 114 19, Sweden

9 ⁴ Abisko Scientific Research Station, Swedish Polar Research Secretariat, Abisko, 981 07, Sweden

10 ⁵ Centre for Environmental and Climate Science, Lund University, 223 62, Sweden

11

12 Correspondence to: Patryk Łakomic (patryk.lakomic@nateko.lu.se)

13

14 **Abstract**

15 The Arctic is exposed to even faster temperature changes than most other areas on Earth.
16 Constantly increasing temperature will lead to thawing permafrost and changes in the methane
17 (CH₄) emissions from wetlands. One of the places exposed to those changes is the Abisko-
18 Stordalen Mire in northern Sweden, where climate and vegetation studies have been conducted
19 from since the 1970s.

20 In our study, we analyzed field-scale methane emissions measured by the eddy covariance
21 method at Abisko-Stordalen Mire for three years (2014-2016). The site is a subarctic mire mosaic
22 of palsas, thawing palsas, fully thawed fens, and open water bodies. A bimodal wind pattern
23 prevalent at the site provides an ideal opportunity to measure mire patches with different
24 permafrost statusesstatus with one flux measurement system. The flux footprint for westerly
25 winds is dominated by elevated palsa plateaus, while the footprint is almost equally distributed
26 between palsas and thawing bog-like areas for easterly winds. As these patches are exposed to
27 the same climatic and weather conditions, we analyzed the differences in the responses of their
28 methane emission for environmental parameters.

29 The methane fluxes followed a similar annual cycle over the three study years, with a gentle rise
30 during spring and a decrease during autumn and with no, without emission burst at either end
31 of the ice-free season. The peak emission during the ice-free season differed significantly for the
32 mire with two permafrost statusesstatus: the palsa mire emitted 2419 mg-CH₄C m⁻² d⁻¹ and the
33 thawing wet sectorsector40 mg-C m⁻² d⁻¹. Factors controlling the methane emission were
34 analyzed using generalized linear models. The main driver for methane fluxes was peat
35 temperature for both wind sectors. Soil water content above the water table emerged as an
36 explanatory variable for the three years for western sectors and the year 2016 in the eastern

Formatted: English (United States)

Formatted: Font: 11 pt, English (United States)

Formatted: English (United States)

Formatted: Font: (Default) +Body (Calibri)

Formatted: Font: (Default) +Body (Calibri)

Formatted: Font: (Default) +Body (Calibri)

Formatted: Font: (Default) +Body (Calibri)

Formatted: Font color: Auto

37 sector. ~~Water~~The water table level showed a significant correlation with methane emission for
38 the year 2016 as well. Gross primary production, however, did not show a significant correlation
39 with methane emissions.

40 Annual methane emissions were estimated based on four different gap-filing methods. The
41 different methods generally resulted in very similar annual emissions. The mean annual emission
42 based on all models was $4.23.1 \pm 0.43$ g-CH₄C m⁻² a⁻¹ for the western sector and $7.35.5 \pm 0.75$ g-
43 CH₄C m⁻² a⁻¹ for the eastern sector. The average annual emissions, derived from ~~this~~these data
44 and a footprint climatology, were $3.62.7 \pm 0.75$ g-CH₄C m⁻² a⁻¹ and $11 \pm 8.2 \pm 1.5$ g-CH₄C m⁻² a⁻¹
45 for the palsa and thawing surfaces, respectively. Winter fluxes were relatively high, contributing
46 27 - 45 % to the annual emissions.
47

Formatted: Font: (Default) +Body (Calibri)

Formatted: Font: (Default) +Body (Calibri)

48 1 Introduction

49 After a period of stabilization in the late 1990s to early 2000s, atmospheric methane (CH₄)
50 concentration is increasing again at rates similar to those before 1993, which is approximately
51 12-ppb yr⁻¹ (Dlugokencky et al. 2011, Nisbet et al. 2014, Saunio 2020). The reasons behind this
52 increase are ~~not clearly understood~~still partly unclear, as the mechanisms that control the global
53 CH₄ budget are not completely ~~comprehended~~understood (Kirschke et al. 2013, Saunio et al.
54 2020). The largest natural source of CH₄ ~~is~~are wetlands, based on top-down emission estimates
55 (Saunio et al. 2020), and this source may ~~be~~ become stronger in the warming climate (Zhang et
56 al. 2017). The shift in the isotopic composition of CH₄ towards more negative values also supports
57 the hypothesis of changes in the biological source strength driving the increase in ~~methane~~CH₄
58 concentration, as atmospheric CH₄ is becoming more ¹³C-depleted (Nisbet et al. 2016).

Formatted: Font: (Default) +Body (Calibri)

59 Increasing temperature has shown to speed up the degradation of permafrost which leads to
60 losses in the soil carbon pool, often in the form of carbon dioxide (CO₂) and CH₄ (Malmer et al.
61 2005). The high northern latitudes are experiencing the fastest temperature increase due to the
62 ongoing global warming. Temperature changes in the Arctic have been twice as high as the global
63 average (Post et al. 2019).

64 Ecosystems near the annual ~~0°C~~near-surface air temperature isotherms ~~of 0 °C~~ are vulnerable to
65 permafrost thaw and changes in ecosystem characteristics in a warming climate. These
66 vulnerable ecosystems include palsa mires, such as Stordalen Mire near Abisko, Sweden, where
67 the recent warming has led to annual average temperatures exceeding 0 °C since ~~1998~~1980s
68 (Callaghan et al. 2010, Callaghan et al. 2013, Post et al. 2019, Figure S1). The warming has led to
69 an acceleration of permafrost thaw processes and a transition from palsa plateaus, underlain by
70 permafrost, to non-permafrost fen systems (Malmer et al. 2005). These deviations are likely to
71 induce changes in biogeochemical processes, including increased CH₄ emissions (Christensen et
72 al. 2003).

73 The most direct micrometeorological field-scale method used to measure CH₄ exchange between
74 ecosystem and atmosphere is the eddy covariance (EC) method (e.g. Verma et al. 1986, Aubinet
75 et al., 2012). The advantages of this method are its high temporal resolution and minimal

76 disturbance to the measured surface. Thus, it is feasible for long-term measurements of rates of
77 gas exchange that integrates over surface variation (Knox et al. 2016, Li et al. 2016, Rinne et al.
78 2018). However, information on the small-scale spatial distribution of surface fluxes is lost with
79 the method due to the spatially integrative nature of the EC method. Instead of resolving the
80 small-scale spatial variability, the EC method provides averaged fluxes from a larger area, the flux
81 footprint area (Kljun et al. ~~2015~~2002). However, spatial variability can be resolved by the EC
82 method using measurements conducted under different wind directions, as the footprint area is
83 located upwind of the measurement tower. We can take advantage of this feature to obtain gas
84 exchange rates from two different ecosystem types with one measurement system by placing
85 the measurement system on the border between these systems (e.g. Jackowicz-Korczyński et al.,
86 2010; Kowalska et al., 2013; Jammot et al., 2015; 2017). Stordalen Mire offers an excellent
87 opportunity to conduct flux studies where one flux system is used to monitor two ecosystem
88 types since the wind direction is bimodal. While previous studies in the area have compared open
89 water surfaces to completely thawed fen (Jammot et al., 2015, 2017, Jansen et al. 2020), no
90 comparison of field-scale CH₄ emission between permafrost palsa plateaus and thawing wet
91 areas has been conducted yet.

92 Previous studies on CH₄ emission within the Stordalen Mire from areas with different permafrost
93 ~~statuses~~status have been done by using chamber measurements (McCalley et al. 2014, Deng et
94 al. 2014). McCalley et al. (2014) reported CH₄ emissions from palsa underlain by permafrost to
95 be close to zero, summertime emissions from thawing wet areas to be around ~~3525~~ mg-CH₄C m⁻²
96 d⁻², while completely thawed fen sites revealed much higher emission of ~~210150~~ mg-CH₄C m⁻²
97 d⁻². There are only ~~a~~ few wintertime data on CH₄ emission available using the chamber method
98 (Christensen et al. 2000, Nilsson et al. 2008, Godin et al. 2012, McCalley et al. 2014). However,
99 EC measurements conducted at different northern mires typically show low but positive
100 emissions in winter (Rinne et al., 2007; Yamulki et al. 2013, and others).

101 In this study we analyzed field-scale CH₄ emission from two areas of Stordalen subarctic mire.
102 The first area is dominated by ~~drained~~ permafrost plateau, ~~while the~~ The second ~~one~~area is
103 thawing, ~~and thus resulting in~~ wetter ~~areas-conditions~~. Outputs from this analysis are
104 differences in the CH₄ emissions from the mire patches with heterogeneous permafrost status.
105 We are expecting, based on the previous studies, that fluxes from the wetter sector will be
106 around ~~4030~~ mg-CH₄C m⁻² d⁻², while the palsa plateau will emit significantly lower fluxes during
107 at the peak season. We presume that winter fluxes will be positive but very low.

108
109 For estimation of annual CH₄ emission we need gap-free ~~data sets~~ As datasets. Up to date, there
110 at the moment exists no generally accepted gap-filling method for ~~methane~~CH₄ fluxes, hence
111 four different gap-filling methods were compared. ~~All of these methods are uncertain and dealing~~
112 ~~with the gaps differently~~. ~~Test~~The test of the four methods will decrease the uncertainty in an
113 annual balance estimation- (Hommeltenberg et al. (2014), Rößger et al. (2019), Kim et al. (2019)).
114 It was important to use more than one method in this case of study because datasets were
115 ~~portioning~~ portioned and due to that contained more gaps.

Formatted: Font: (Default) +Body (Calibri)

Formatted: Default, Left

Formatted: Font: (Default) +Body (Calibri), 11.5 pt

Formatted: Font: (Default) +Body (Calibri)

116 This study aimed to estimate the annual CH₄ emission from two distinct different ecotypes, with
117 heterogeneous permafrost status, exposed to the same environmental factors. Furthermore, we
118 analyzed the seasonal cycle of CH₄ emission to quantify the contribution during different seasons.
119 Moreover, an analysis of differences in controlling factors for these two different areas ~~will be was~~
120 done.
121

122 2 Materials and method

123 2.1 MeasurementStudy site

124 The study area is Stordalen Mire, a mire complex underlain by discontinuous permafrost located
125 in northern subarctic Sweden (68°20' N, 19°30' E) near Abisko (Åbeskovvu). The station Abisko-
126 Stordalen (SE-Sto) is a part of the ICOS Sweden research infrastructure and is the only one in
127 Sweden situated in the subarctic region ~~in Sweden~~. The measurement period that is analyzed
128 here covers three years from 2014 to 2016. The mean annual near- surface air temperature in
129 this region has been increasing during the last decades, and temperatures recorded by SMHI
130 (Sveriges meteorologiska och hydrologiska institut) at ANS (Abisko Naturvetenskapliga Station)
131 has exceeded the 0°_C threshold since the late 1980s (Callaghan et al. 2013, Figure S1). During
132 the years 2014-2016, the mean ~~annual~~near-surface air temperature (Ta) was 1.~~030~~ °C and 0.~~273~~
133 °C at ANS and the ICOS Sweden station Abisko-Stordalen (SE-Sto), respectively. The average
134 annual precipitation, based on ANS data, is around 330_mm-yr⁻¹. An acceleration of permafrost
135 loss with increasing temperatures is likely (Callaghan et al. 2013).

136 The large mountain valley of Lake Torneträsk (Duortnosjávri) channels winds at the
137 ~~measurementstudy~~ site, leading to a bimodal wind distribution (Figure 1)~~that~~, which allows us
138 to divide our analyses into two distinct sectors. The plant community structure around the tower
139 is determined by the hydrology which in turn is determined by the microtopographic variation in
140 the surface due to the local permafrost dynamics. Different plant communities would have
141 different productivities thus controlling the CO₂ and CH₄ fluxes from those surfaces. The area to
142 the west of the EC mast is dominated by a drier permafrost palsa plateau hereafter referred to
143 as the western sector, whereas the area to the east is a mixture of thawing wet areas and palsas,
144 hereafter referred to as the eastern sector. The drained permafrost plateau is dominated by
145 *Empetrum hermaphroditum*, *Betula nana*, *Rubus chamaemorus*, *Eriophorum vaginatum*,
146 *Dicranum elongatum*, *Sphagnum fuscum*. The wet areas are characterizing by *E. vaginatum*,
147 *Carex rotundata*, *S. balticum*, *Drepanucladus schulzei*, *Politrichum jensenii* (Johansson et al.
148 2006). The thawing areas in this sector exhibit ombrotrophic, bog-like, features. Dominant
149 vegetation varies with the microforms of the mire.

150

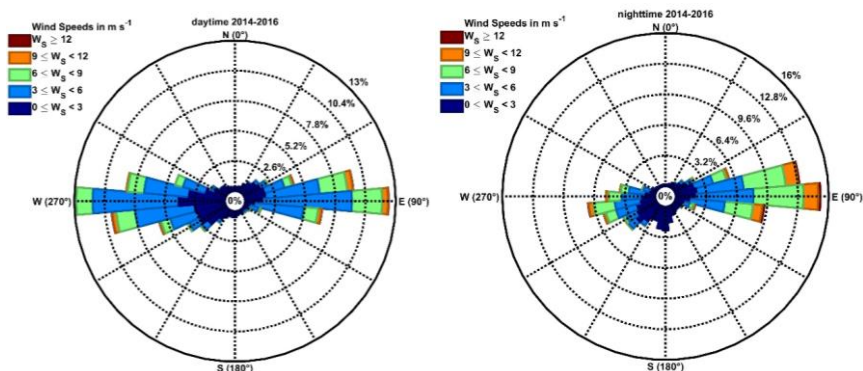
151

152

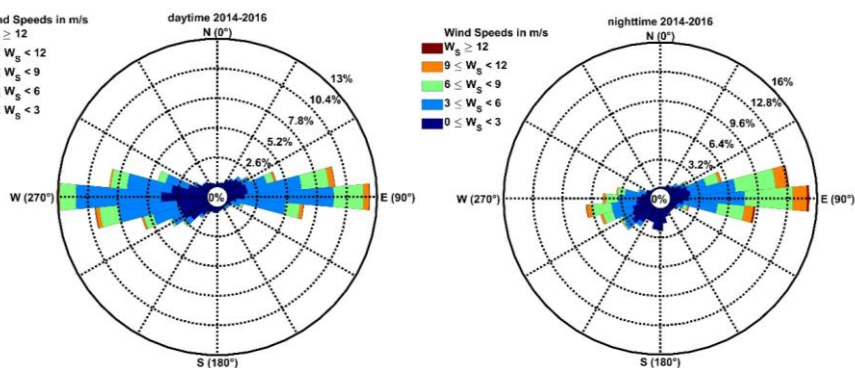
Formatted: Font: (Default) +Body (Calibri)

Formatted: Font: 11 pt

Formatted: Space After: 8 pt, Line spacing: Multiple
1.08 li, Adjust space between Latin and Asian text,
Adjust space between Asian text and numbers



153
 154 Figure 1. The wind rose for SE-Sto tower for years 2014-2016 for the daytime (left panel) and nighttime
 155 (right panel)



156
 157

158 2.2 Flux measurements

159 The EC measurements of CH₄ fluxes at SE-Sto are made using a ~~close~~closed-path fast off-axis
 160 integrated cavity output spectrometer (OA-ICOS LGR model GGA-24EP, ABB Ltd, Zurich,
 161 Switzerland) combined with a 3-D sonic anemometer (SA-Metek uSonic-3 CLASS A, Metek GmbH,
 162 Germany). Air was sampled via a 29.6 m long polyethylene tubing with an 8.13 mm inner
 163 diameter. Analysis of the high-frequency loss were performed to assess the effect of relatively
 164 long sample tubing. We analyzed this with the co-spectra of the CH₄ and the vertical wind speed
 165 w. The analysis did not show a dampening effect at the high frequencies (Figure S2), thus the high
 166 frequency attenuation does not seem to be very large. Furthermore, the post-processing
 167 software we used to calculate fluxes includes correction for high-frequency losses. The nominal
 168 tube flow rate was 36 l min⁻¹. The sampling inlet was displaced 22 cm horizontally of the sonic
 169 anemometer measurement volume towards 180°. The response time of the LGR-FGGA was 0.1 s.

Formatted: Font: (Default) +Body (Calibri)

Formatted: Default

170 The LGR FGGA was placed inside a heated and air-conditioned shelter. The anemometer was
171 located north of the instrument shelter and was oriented with the sensors north pointing towards
172 186°. This orientation allows undisturbed wind measurements from both main wind directions,
173 East and West.

174 CO₂ and H₂O were measured with ~~LiCor~~ LI-COR LI-7200 (~~LI-COR~~ LI-COR Environment, USA) closed
175 path infra-red gas analyzer. The sampling inlet was at the same location as the sampling point for
176 the CH₄ analyzer. Sampled air was transported through 1.05 m and of 5.3 mm ID tubing. The
177 nominal tube flow rate was 15 l min⁻¹.

178 The anemometer and air sampling tubes were mounted on a mast of 2.2 m above ground level
179 (a.g.l.) (68°21'21.32" N, 19°-2'42.75" E), placed ~~on~~ at the edge of the western and the eastern
180 sectors. Data were collected by an ISDL data logger (In Situ Instrument AB, Sweden) with a 20 Hz
181 time resolution.

182

183 2.3 Ancillary Measurements

184 Ancillary measurements are presented in Table S1. The sampling frequency for these parameters
185 was 1 Hz and the collected data were averaged into half-hourly values. Measured variables are
186 divided into two categories: peat/soil parameters, and meteorological parameters. Peat
187 temperatures at each depth, soil heat fluxes, and soil water contents (SWC) were measured at
188 four ~~plots~~ locations around the EC tower, located towards the four cardinal directions. In further
189 analysis, data just from two of these locations were used (East and West) as these were within
190 the flux ~~footprints~~ footprint areas of the EC tower. The sites for the water table level (WTL)
191 measurements differed from the peat temperature profiles. The soil pit for temperature and
192 moisture probe in the western sector is located on a palsa plateau. However, the WTL probe is
193 located in a pond approximately 10 m away from the soil temperature and SWC measurement,
194 as there is no WTL above the permafrost of palsas. The soil pit for temperature and SWC probe
195 in the eastern sector is located in the wet thawing area. The WTL probe is located in the wetter
196 area approximately 10 m away. Furthermore, data for WTL was available only during the
197 unfrozen period, as the probes were removed during the frozen period to avoid damage. ~~The~~
198 ~~WTL on the western sector was measured in a wet collapse feature, surrounded by drained areas.~~
199 ~~The palsa areas commonly have no persistent WTL above the permafrost surface.~~ Meteorological
200 variables were measured on a separate mast, placed 10 meters south-west of the flux
201 measurement mast.

202

203 2.4 Flux calculation

204 Fluxes of CO₂, CH₄, H₂O, and sensible heat were calculated using EddyPro 6.2.1 (~~LI-COR~~ LI-COR
205 Environment, USA) as half-hourly averages. The data quality flagging system and advanced
206 options for EddyPro were set up following Jammet et al. (2017). The wind vector was rotated by

Formatted: Font: (Default) +Body (Calibri)

Formatted: Font color: Auto

Formatted: Font: (Default) +Body (Calibri)

207 a double rotation method and data were averaged by block averaging (Aubinet et al. 2012). The
208 time lag was obtained by maximizing the covariance (Aubinet et al. 2012).

209 Based on the wind direction, the half-hourly data were divided into western and eastern datasets,
210 similarly to analyses by Jackowicz-Korczyński et al. (2010) and Jammet et al. (2015, 2017). The
211 eastern dataset contained fluxes and other variables recorded when the wind was from 45° -
212 135° , and the western dataset parameters when wind directions were 225° - 315° . These two
213 datasets were analyzed separately. Fluxes measured with wind from these two sectors are
214 influenced by mire surfaces dominated by differing permafrost status, moisture regimes, and
215 plant community structures. These reflect the thaw stages of a dynamic arctic land surface,
216 responding to the warming climate. These two wind sectors ~~cover~~include more than 80 % of all
217 data during the years 2014-2016. Northerly and Southerly wind directions, i.e. winds from
218 outside these sectors occurred mainly in low wind speed conditions. The distribution of wind
219 directions is presented in Figure 1.

220 CH₄ fluxes were filtered by quality flags according to Mauder and Foken (2004). These indicate
221 the quality of measured fluxes, "0" being the best quality fluxes, "1" being usable for annual
222 budgets, and "2" being flux values that should not be used for any analysis. Thus, in further
223 analysis fluxes with flag "2" were removed. Also, ~~flux values when two consecutive~~ data points
224 ~~originated~~originating from ~~different~~the two pre-defined wind direction sectors were removed ~~to~~
225 ~~avoid influences from non-stationary conditions~~. We also analyzed the behavior of the CH₄ fluxes
226 against low turbulence conditions using friction velocity (u^*) as a measure of turbulence. We
227 binned the CH₄ fluxes into $0.05 \text{ m s}^{-1} u^*$ bins and plotted the binned CH₄ flux values against u^* in
228 40-day windows over the growing period (d.o.y. 150-250, d.o.y. 210 was the beginning of the last
229 averaging window). The CH₄ flux showed no dependence on u^* below 0.6 m s^{-1} . A slight positive
230 correlation was found during stronger turbulent conditions ($u^* > 0.6 \text{ m s}^{-1}$), but we deemed this
231 not high enough to warrant exclusion of those points from further analysis. Thus, we ~~removed~~
232 ~~and did not remove~~ data based on the results of u^* . The fraction of data remaining, after filtering
233 based on the quality flags and other criteria described above, is presented in Table 32.

234 The analysis of relations of CH₄ fluxes to environmental parameters was done using ~~the~~ non-gap-
235 filled dataset of daily averages, to avoid the danger of circular reasoning of analyzing the relations
236 to the same factors that were ~~be~~used for gap-filling.

237

238 2.5 Footprint modeling and land cover classification

239 ~~Footprint calculation was made with the model described by Klijn et al. (2015). Receptor height,~~
240 ~~Obukhov length, a standard deviation of lateral velocity fluctuations, friction velocity, and~~
241 ~~roughness length were used as input data. The input data were divided into the two sectors~~
242 ~~mentioned above, before footprint calculation, and footprints were calculated separately for~~
243 ~~them. We calculated footprints for each half hourly data point and aggregated these to annual~~
244 ~~footprint climatologies for each sector separately.~~

Formatted: Font: 11.5 pt, Pattern: Clear

Formatted: Font: 11.5 pt, Pattern: Clear

Formatted: Font: 11.5 pt, Pattern: Clear

Formatted: Font: 11.5 pt, Pattern: Clear

Formatted: Font: (Default) +Body (Calibri)

245 A detailed land cover classification was performed ~~overfor~~ the EC-tower footprint area to
246 estimate the flux contribution from the drained palsa and the thawing wet areas. We used images
247 over the Stordalen Mire collected with an eBee (SenseFly, Lausanne, Switzerland) Unmanned
248 Aerial Vehicle (UAV) carrying a Parrot Sequoia camera (Parrot Drone SAS, Paris, France) on July
249 31, 2018. The images were processed in Agisoft Photoscan (Agisoft LLC, St. Petersburg, Russia) to
250 create an orthomosaic and a Digital Surface Model (DSM) with spatial resolutions of 50 cm x 50
251 cm. Field data for training a classification were collected in mid-August 2018 with sampling areas
252 of 50 cm x 50 cm that were classified into wet or dry, and a random forest classification was
253 performed to classify the footprint into wet and dry areas with the orthomosaic and DSM as
254 input. The dry areas in the flux footprint areas of SE-Sto footprint correspond to palsas, while the
255 wet areas are thawing surfaces.

256 Flux footprints were calculated with the FFP model (Kljun et al. 2015). Receptor height, Obukhov
257 length, standard deviation of lateral velocity fluctuations, friction velocity, and roughness length
258 were used as input data. The input data were divided into the two wind sectors mentioned above,
259 before footprint calculation, and footprints were calculated separately for them. We calculated
260 footprints for each half-hourly data point and aggregated these to annual footprint climatologies
261 for each sector separately. I.e. the half-hourly footprint function values were aggregated for each
262 land cover grid cell (50 cm x 50 cm) to derive a footprint-weighted flux contribution per pixel.

263 Based on the land cover classification and annual CH₄ fluxes for each sector, combined and
264 weighted with the footprint ~~climatology~~climatology, it was possible to estimate annual emissions
265 from the different surface type.

266

267 2.6 Gap-filling methods for CH₄

268 We compared four different gap-filling methods, separately for both sectors. These methods
269 were: look-up tables (REddyProc (“Jena gap-filling tool”), Wutzler et al. 2018), 5-day moving
270 mean, artificial neural network (Jammert et al. 2015, 2017), and generalized linear models (Rinne
271 et al. 2018). All these methods, except for moving mean, have been used before for gap-filling
272 CH₄ flux data from different mire ecosystems. The look-up table approach uses half-hourly data,
273 while for the other three methods we used daily average data, as ~~methane~~CH₄ emissions from
274 this ecosystem do not show a diel cycle (See see below, ~~chapter~~Section 3.2 for a detailed
275 description).

276 The uncertainties due to each method were analyzed by the introduction of artificial gaps to the
277 data, with lengths comparable to gaps existing in the year 2014. 35-day and 80-day gaps were
278 implemented to the data of years 2015 and 2016. Gaps were placed in the winter period, to
279 obtain similar gap distribution as in the year 2014 (gap distribution is presented below in Table
280 4.3). Annual sums, with artificial gaps, were compared with results from methods without those
281 gaps. Statistical significances of differences between models were analyzed by using a two-
282 sample t-Test for equal means with a 95 % confidence level (MATLAB R2019b).

Formatted: Font: (Default) +Body (Calibri)

283

284 [2.6.1 REddyProc](#)

285 The Jena gap-filling tool using look-up tables requires half-hourly data of CH₄ flux and
286 environmental data: ~~global~~shortwave incoming radiation, air temperature, soil temperature,
287 relative humidity, and friction velocity. Based on environmental data, fluxes are classified and
288 averaged within a given time window. The missing data are then filled with the average value
289 from classified data. Uncertainty can be estimated as standard deviations of fluxes within classes.
290 Detailed information about the method is presented by Falge et al. (2001) and Wutzler et al.
291 (2018).

Formatted: Font: (Default) +Body (Calibri)

292

293 [2.6.2 Moving average](#)

294 A 5-day moving mean approach is a very simple gap-filling method where the moving mean is
295 calculated for subsets of the data. In case of a gap in the ~~number of observations in the~~-averaging
296 window, the mean value is calculated for ~~the fewer numbers of points~~observations. The method
297 was applied on daily average CH₄ flux data using MATLAB (movmean function). For gaps longer
298 than 5 days, linear interpolation was used between the last point before the gap and the first
299 point after gap. Uncertainties of the single gap-filled flux were estimated by calculating the
300 moving standard deviation (movstd function, MATLAB) on the same subset of the data like for
301 the moving mean.

Formatted: Font: (Default) +Body (Calibri)

302

303 [2.6.3 Artificial Neural Network](#)

304 An artificial neural network (ANN) has been successfully applied for gap-filling of CH₄ fluxes by
305 e.g. Dengel et al. (2013), Jammet et al. (2015,2017), ~~and~~-Knox et al. (2016), ~~and~~ Rößger et al.
306 (2019). This type of ANN was designed in MATLAB using a fitnet function with 30 hidden neurons.
307 We used the Levenberg-Marquardt algorithm as a training function (Levenberg 1944 Marquardt
308 1963). All available daily average CH₄ values were used to train (70 %), validate (15 %), or test (15
309 %) the ANN. The ANN requires input data without gaps to work properly and thus the short gaps
310 (up to three days) in environmental daily averaged data were filled by linear interpolation before
311 the ANN analysis. All environmental variables, except ~~for~~ the WTL were used as input for the ANN
312 method. The WTL was excluded because it was not available during the frozen period, i.e. most
313 of the year. -The ANN method was applied to sectors and each year separately (ANN YbY) or all
314 three years together. Multiple repetitions were done to minimize uncertainty connected with
315 randomly chosen data points for training, validation, and testing. The network was trained and
316 used to calculate the time series of CH₄ daily fluxes 100 times in each case of gap-filling. The
317 number of repetitions was chosen to have a sample large enough to calculate reliable mean and
318 standard deviation values, and to keep the computation time reasonably short. An average CH₄
319 flux for each day was calculated based on 100 daily values. The gaps in the measured flux time

Formatted: Font: (Default) +Body (Calibri)

Formatted: Font: (Default) +Body (Calibri)

320 series were filled with values from the time series calculated by ANN. Errors were estimated as
321 standard errors of mean on daily flux, based on 100 ANN trained values.

322

323 2.6.4 Generalized Linear Model

324 Generalized linear models (GLM) are linear combinations of linear and quadratic functions
325 describing the dependence of response variables to predictors. In our case, the response variable
326 was the logarithm of daily average CH₄ flux, and predictors were daily averages of measured
327 environmental variables. Controlling factors of CH₄ emission were examined by a procedure
328 similar to the routine described by Rinne et al. (2018). A correlation matrix of linear correlation
329 based on daily values of environmental factors and CH₄ fluxes was constructed (Figure S2S3).
330 Additionally, the logarithm of CH₄ fluxes was added to the correlation matrix to check the
331 exponential relationship between parameters. This type of relationship between CH₄ fluxes and
332 peat temperature was previously found by e.g. Christensen et al. (2003), Jackowicz-Korczyński et
333 al. (2010), Bansal et al. (2016), Pugh et al. (2017) and Rinne et al. (2018). Gap-filled CO₂ flux, and
334 gross primary production (GPP), were also included as prospective controlling factors. In order to
335 avoid strong cross-correlation between predictors, first, we selected the parameter with the
336 highest correlation and then removed parameters from the GLM development with a cross-
337 correlation between parameters $R^2 > 0.6$. We thus chose GPP, soil temperature at 30 cm depth
338 for the eastern sector and 10 cm depth for the western sector, soil water content (SWC), short-
339 wave incoming radiation, and vapor pressure deficit (VPD) as possible predictors. The model was
340 constructed in MATLAB using the stepwiseglm function (Dobson 2002). The GLM was made for
341 both separately for each year (GLM YbY) and for all three years combined. Errors were
342 estimated as 95 % confidence intervals because it was an output of the stepwise function. This
343 method was also used for the determination of the controlling factors from the possible
344 predictors.

345

346 2.7 Gap-filling of CO₂ fluxes

347 CO₂ fluxes were calculated for the two both wind sectors. CO₂ flux exhibited the diel pattern in
348 the growing season, with uptake during daytime (Global shortwave incoming radiation > 50 W m⁻²)
349 and release at night (Global shortwave incoming radiation < 50 W m⁻²). We used the ANN to
350 gap-fill the time series of CO₂ fluxes. This method was chosen to check the possibility of
351 reconstruction to reconstruct the diel cycle. This diel pattern of CO₂ was taken into account by
352 using half-hourly data. We used all environmental variables excluding the WTL, as for CH₄ fluxes.
353 GPP was obtained by partitioning the gap-filled data using the Jena gap-filling tool. Finally, the
354 half-hourly gap-filled GPP and CO₂ data were averaged to daily values.

355

Formatted: Font: (Default) +Body (Calibri)

Formatted: Font: (Default) +Body (Calibri)

2.8 Contribution of palsa and thaw surfaces to average CH₄ emission

Using the average annual CH₄ emission from the two wind sectors and the relative contributions of the two surface types to the fluxes from these sectors, we ~~could calculate~~calculated the average annual emission from these surface types. We ~~could express~~expressed the average annual CH₄ ~~flux~~fluxes for the two sectors, F_e (East) and F_w (West), with a pair of equations,

$$F_e = f_{e,p}E_p + f_{e,t}E_t, \quad (1)$$

$$F_w = f_{w,p}E_p + f_{w,t}E_t, \quad (2)$$

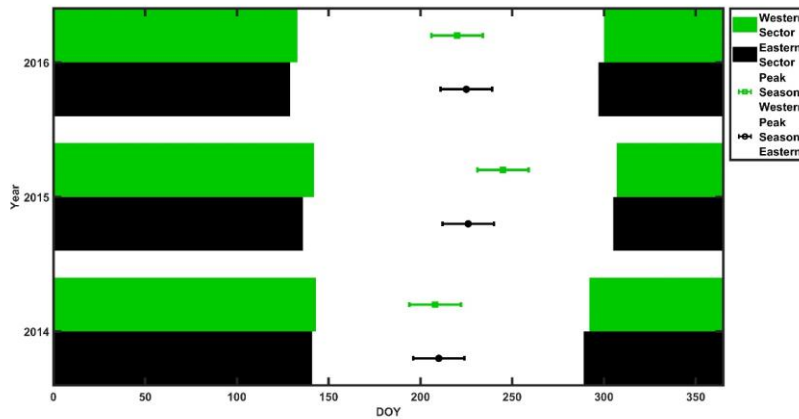
where f indicates the fractional contribution of surface type to the flux from the footprint calculations (subscripts e and w referring to east and west, respectively; ~~and~~ p and t to palsa and thaw surface, respectively); and E_p and E_t are emissions from palsa and thaw surface, respectively. We ~~could solve~~solved this equation set with two unknowns to yield E_p and E_t . Here we assumed that the emission rate from both palsa and thaw surfaces are equal in eastern and western sectors. Furthermore, we must assume that there is no correlation between footprint contribution and seasonally developing emission rate at either surface type. The seasonally constant contributions of the surface types to the footprint indicate that the latter assumption may well be valid (Figure S4).

2.9 Definition of seasons

The beginning of the unfrozen period was defined as the day when daily averages of peat temperature at 10 cm depth had been above 0°C for three consecutive days. The end of the unfrozen period was defined as the day when daily averages of peat temperature at 10 cm depth had been below 0°C for three consecutive days. The unfrozen and frozen periods commence in the western sector on average 3 days earlier than in the eastern sector, but differences in the unfrozen season length are not systematic (Table 1Figure 2). The beginning and the end of the unfrozen season ~~for both sectors~~were determined independently for both sectors. The horizontal distance between soil temperature sensors in eastern and western sectors was around 75 m, differed about 2 m elevations in elevation, and ~~were roughly 40 m~~the distance from the flux tower was roughly 40 m.

Formatted: Font: (Default) +Body (Calibri)

Formatted: Font: (Default) +Body (Calibri)



386
 387 Figure 2. Time periods of frozen peat during the years 2014 - 2016 (green and black bars) and
 388 peak CH₄ emission season (dot with whiskers) for the western sector (green) and the eastern
 389 sector (black). (For peak season definition see Section 3.2)

390

391 3 Results

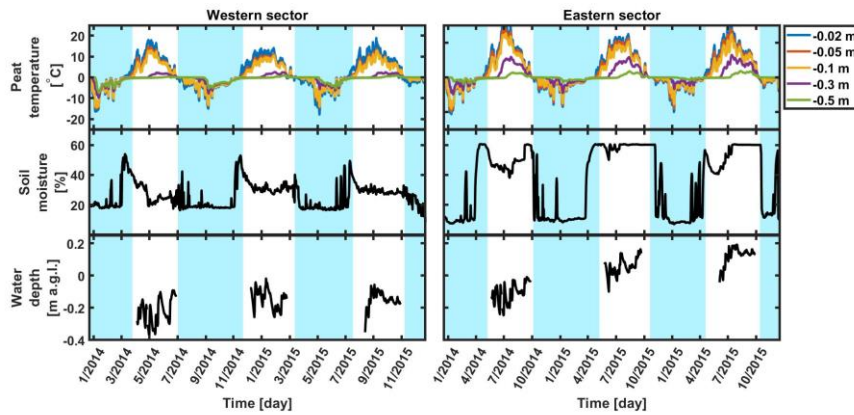
392 3.1 Environmental conditions and flux footprints

393 Winds from eastern and western sectors contributed to 50 % and 40 % to the daytime wind
 394 directions, respectively (Figure 1). Northerly and southerly winds contributed to around 5 % each.
 395 In the nighttime, 51 % of wind was from the East and 32 % from the West. Additionally, 15 % of
 396 total wind came from the South during nighttime, probably as catabatic flow from higher
 397 mountain areas. The wind from North was rare, around 2 % of all the cases.

398 The annual average peat temperature of the uppermost 50 cm of peat was systematically warmer
 399 in the eastern sector than in the western sector (Table 21; Figure 23). However, the summertime
 400 peat temperature at the top 10 cm layer was warmer for the western sector (Figure 335). The
 401 situation was the opposite during winter when the western sector down to 50 cm was colder
 402 than the eastern sector. The During our investigation period (2014-2016), the peat temperatures
 403 from 30 cm to 50 cm below ground were colder in the western sector, was colder than those of
 404 the eastern sector, causing corresponding to the existence of the permafrost. Temperature
 405 differences, between both areas, at the same depth, were stable over the measurement years.
 406 The biggest difference was noticed at a depth of 30 cm. The temperature temperatures at 30 cm
 407 and 50 cm depth was were increasing during consecutive years.

408

Formatted: Font: (Default) +Body (Calibri)



409
410
411
412
413
414

Figure 23. Time series of daily mean values for western and eastern sectors for: peat temperature (top panel), soil moisture (middle panel), and water table level (bottom panel), where the shaded light blue area is the frozen period, when peat temperature at 10 cm was below 0°C (see chapter Section 2.8 for a detailed description).

Formatted: Font: (Default) +Body (Calibri)

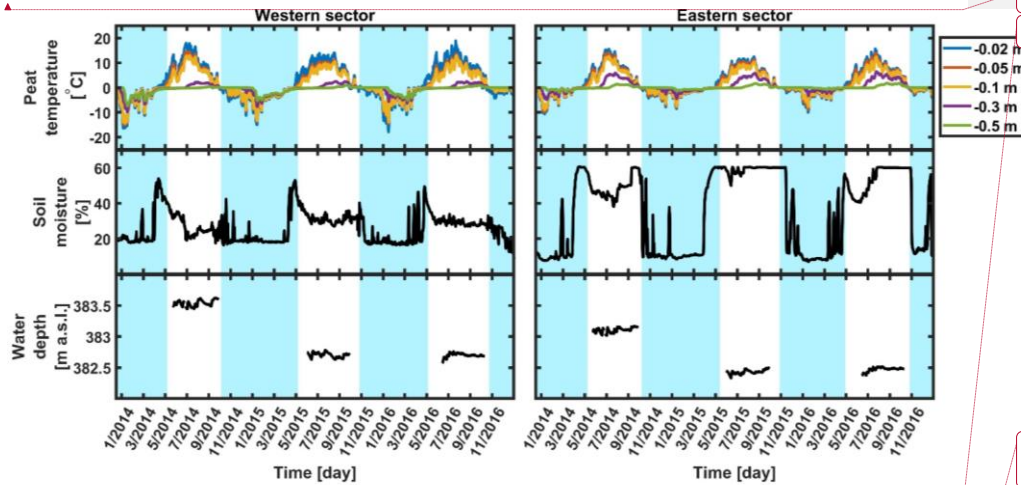
Formatted: Font: (Default) +Body (Calibri)

Formatted: Font: 10 pt

Formatted: Font: 12 pt

Formatted: Font: (Default) +Body (Calibri)

415



416
417

Table 21. Mean annual air and peat and air temperature temperatures for the years 2014-2016 for eastern and western sectors.

Formatted: Font: (Default) +Body (Calibri), Not Bold, Not Italic

Formatted: Font: (Default) +Body (Calibri)

Formatted: Font: (Default) +Body (Calibri), Not Bold, Not Italic, Font color: Auto

Formatted: Font: (Default) +Body (Calibri), Not Bold, Not Italic

Formatted Table

Temperature [°C]

depth in cm	2014 E	2014 W	2014 E-W difference	2015 E	2015 W	2015 E-W difference	2016 E	2016 W	2016 E-W difference
ambient air	0.303	-0.3	-	0.141	-0.1	-	0.353	-0.3	-
2	1.626	1.384	0.242	2.212	1.962	0.252	2.172	1.939	0.242
5	1.374	0.848	0.535	1.959	1.293	0.657	1.939	1.293	0.646
10	1.192	0.545	0.646	1.707	1.051	0.657	1.707	1.401	0.606
30	0.343	-0.889	1.212	0.616	-0.586	1.192	0.828	-0.485	1.303
50	-0.121	-1.097	0.858	-0.040	-0.798	0.758	0.162	-0.656	0.898

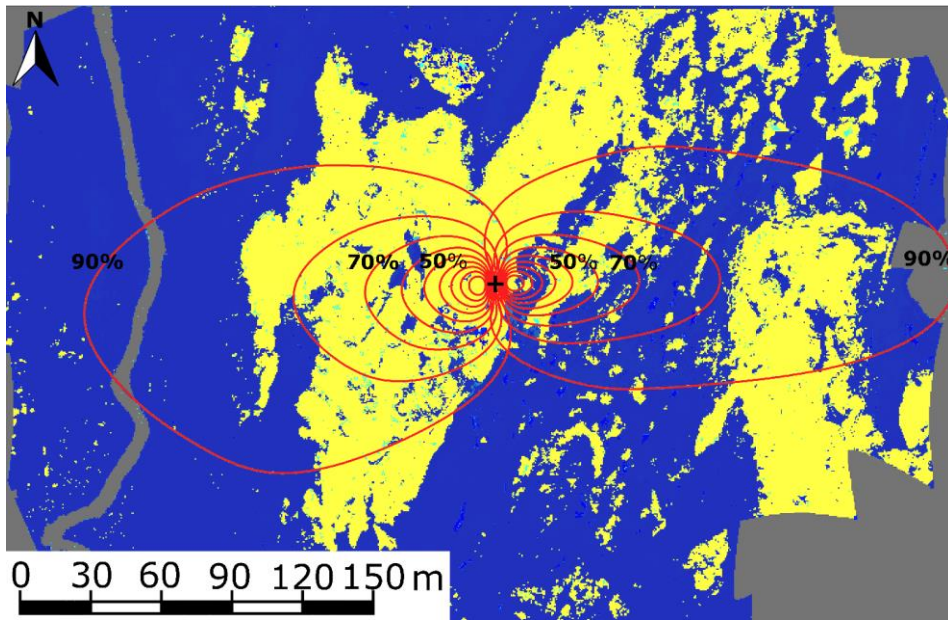
420

421 The WTL was higher in 2014 than in 2015 and 2016 according to measurements both in the
422 eastern and western sectors (Figure 23). This is not reflected in the SWC measurements, which is
423 probably due to the different locations of the measurements of WTL and SWC. In the western
424 sector the WTL was measured in an isolated wet patch, surrounded by drier palsa and thus it is
425 not representative of the dominating type of this area. The WTL in the eastern sector was more
426 representative of the area of the footprint. Data from the WTL probe in the West part of the mire
427 was excluded from the further analysis as it does not represent the situation for the majority of
428 the western sector. The soil moisture was higher for the eastern than the western sector during
429 all years. The data shows a distinctive step change at thaw and freeze, as the dielectricity of ice
430 and liquid water differ. In the eastern sector, the soil was fully saturated for most of the unfrozen
431 period during the years 2015-2016, while 2014 indicates lower water content levels. The western
432 sector was ~~not~~never fully saturated at any time during the years 2014-2016.

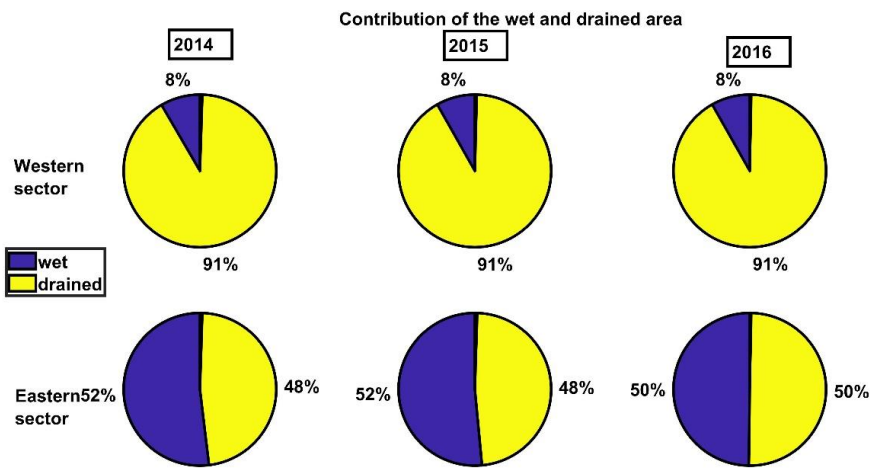
433 Footprint and flux contribution of drier and wetter areas are presented in Figure 3. The dry areas
434 (yellow) contribute on average over all three years to more than 90-% of the fluxes measured
435 from the western sector at the eddy covariance tower. In the eastern sector, the wetter (blue)
436 and drier areas contribute almost equally to the fluxes. The contributions of the wet and dry
437 areas to the fluxes in both sectors ~~were stable~~remained almost constant across the three study
438 years.

439

440



441

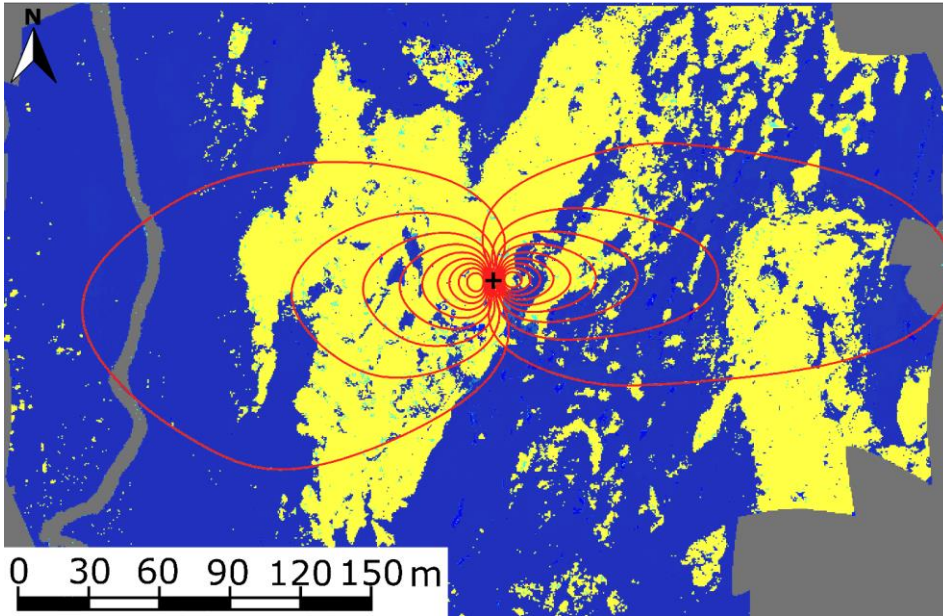


442

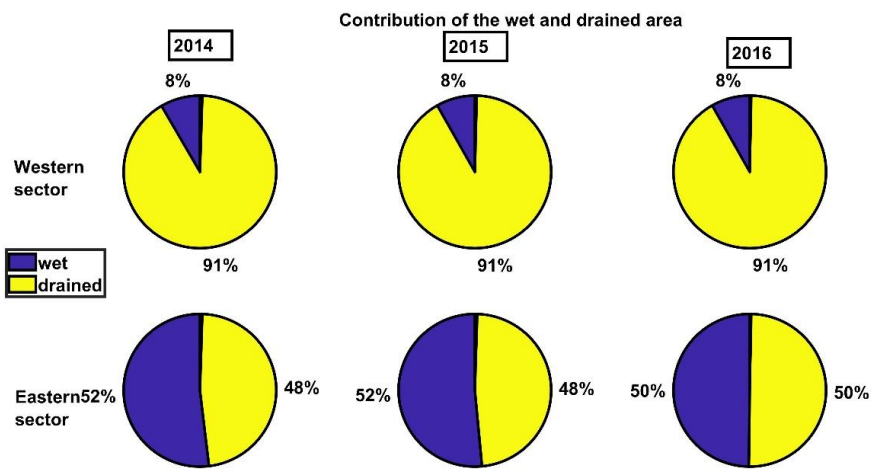
443 Figure 34. Footprint climatology for westerly-weighted contribution of the wet and easterly wind-drained
 444 area at the SE-Sto tower (upper panel) for the year 2014 and relative amounts of wetter areas (blue) and
 445 drained palsa area (yellow) inside the 80 % area of influence of the footprints- (lower panel). The black
 446 cross is the location of the tower and each red line indicates 10 % of the contribution from the source

Formatted: Left

447 area to measured fluxes at the tower. The footprint climatology is almost identical for all study years,
448 see bottom panel.



449



450

451

3.2 CH₄ fluxes

We analyzed during the growing season data of each year and both wind sectors separately in regards to a possible diel cycle of CH₄ fluxes. This was done by normalizing each half-hourly flux by dividing it with the daily median from that day and then calculating the median normalized flux for each half an hour period of the day for the whole growing season (Rinne et al. 2007). This yielded a normalized diel cycle of CH₄ fluxes. As seen in Figure S4, no diel cycle was observed. Thus, Figure S6 shows slightly lower emission during mid-day hours. However, the difference is small compared to the short term variation in the fluxes as indicated by the interquartile range. Thus, for the purpose of gap-filling this effect could be negligible in calculating daily averages. However, it is interesting to observe this type of diel cycle, with minima at daytime. It could be linked to the temperature cycle of the top peat layer. This could affect the methanotrophy, while the methanogenesis occurring at slightly deeper layers would be less affected. This would lead to higher methanotrophy at daytime and thus lower emission. It is possible to calculate CH₄ daily averages without gap-filling the diel cycle, similarly to e.g. Rinne et al., (2007, 2018) and Jackowicz-Korczyński et al. (2010). We discarded daily averages with less than 10 flux data points from further analysis, to ensure the reliability of the daily average fluxes. Uncertainties of daily averages were calculated as standard errors of the mean. The size of the available flux data set, after gap-filling by daily averaging, is presented in Table 32. The gap distribution in the datasets for the different sectors and years is presented in Table 43.

Table 32. The size of available daily data sets after gap-filling by daily averaging for each year and wind sector.

	2014 E	2015 E	2016 E	2014 W	2015 W	2016 W
total number of points	365	365	366	365	365	366
number of points after averaging	137	174	182	96	167	178
% of available data	38	48	50	26	46	49
% of available data during winter period	36	54	56	12	36	37
% of available data during unfrozen period	40	41	42	47	58	63

Table 43. Gaps distribution over years and wind direction.

Type of gap	Length of gap	2014 E	2015 E	2016 E	2014 W	2015 W	2016 W
short gap	1-3 day	32	50	41	24	44	36
medium gap	4-7 day	7	12	11	6	8	11
long gap	8-30 day	3	7	4	4	6	6
very long gap	> 30 day	1	0	0	3	0	0

Formatted: Font: (Default) +Body (Calibri)

Formatted: Font color: Custom Color(RGB(34,34,34)), Pattern: Clear (White)

Formatted: Font: 11 pt, Not Bold, Not Italic

Formatted Table

Formatted: Font: 11 pt, Not Bold, Not Italic

Formatted: Font: 11 pt

Formatted: Font: 11 pt, Not Bold, Not Italic

Formatted: Font: 11 pt

Formatted: Font: 11 pt, Not Bold, Not Italic

Formatted: Font: 11 pt

Formatted: Font: 11 pt, Not Bold, Not Italic

Formatted: Font: 11 pt

Formatted: Font: 11 pt, Not Bold, Not Italic

Formatted: Font: 11 pt

Formatted: Font: (Default) +Body (Calibri), 11 pt, Not Bold, Not Italic

Formatted Table

Formatted: Font: (Default) +Body (Calibri), 11 pt, Not Bold, Not Italic

Formatted: Font: (Default) +Body (Calibri), 11 pt

Formatted: Font: (Default) +Body (Calibri), 11 pt, Not Bold, Not Italic

Formatted: Font: (Default) +Body (Calibri), 11 pt

Formatted: Font: (Default) +Body (Calibri), 11 pt, Not Bold, Not Italic

Formatted: Font: (Default) +Body (Calibri), 11 pt

Formatted: Font: (Default) +Body (Calibri), 11 pt, Not Bold, Not Italic

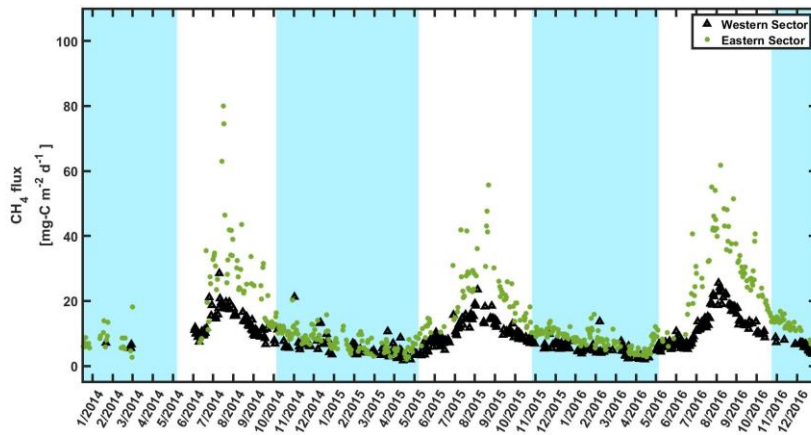
Formatted: Font: (Default) +Body (Calibri), 11 pt

477

478 Daily non-gap-filled CH₄ fluxes showed a characteristic annual cycle, with peak emissions in
479 August (Figure 45) and low but positive wintertime fluxes. These Wilcoxon rank sum test need
480 data without autocorrelation. The autocorrelation in the data existed up to 8 days. Based on this
481 we divided winter data with subsets where every 9th day was selected. We tested the difference
482 of those subsets to zero with Wilcoxon rank sum test. Winter fluxes were statistically different
483 from zero ($p < 0.001$, two-sided Wilcoxon rank sum test). Winter fluxes from the western and
484 eastern sectors were also different from each other ($p < 0.001$).

485 CH₄ fluxes, both from the western sector and the eastern sector started increasing after
486 snowmelt up to ~~the~~ maximum in August (Figure 45). No major springtime emission burst nor
487 autumn freeze-in burst were observed in any of the years.

488



489

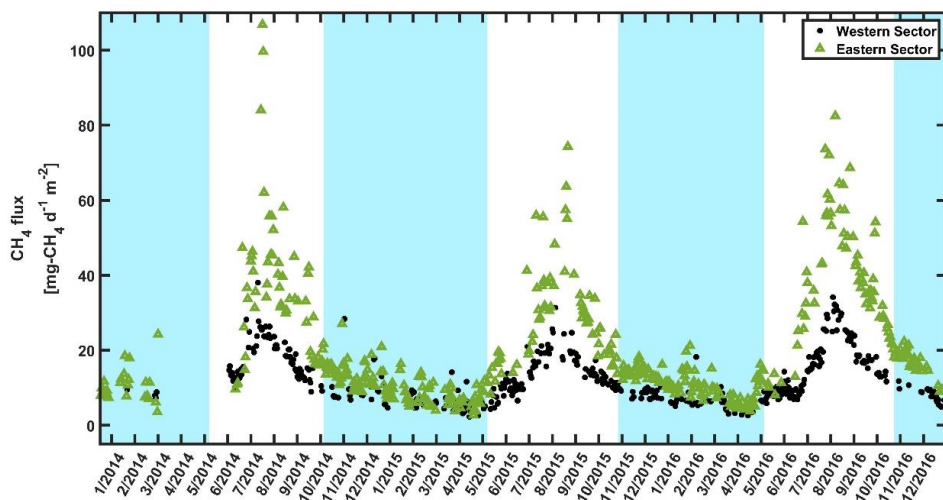
490 Figure 45. Time series for non-gap-filled CH₄ daily averaged fluxes for the western sector (green
491 triangles) and the eastern sector (black dots), where the shaded light blue area is frozen period when
492 peat temperature at 10 cm was below 0°C (see chapterSection 2.8 for a detailed description).

493

Formatted: Font: (Default) +Body (Calibri)

Formatted: Font: (Default) +Body (Calibri)

Formatted: Font: (Default) +Body (Calibri)
Formatted: Justified, Space After: 8 pt, Line spacing:
Multiple 1.08 li



494

495

496 The middle-day of the peak season of the CH₄ emission was defined as the maximum of the
 497 14-days moving average. Two weeks forward and backward from the day with the maximum
 498 daily emission middle-day was defined as the peak season and emissions were estimated for that
 499 period in a given each year. The average emission during the peak seasons was 5640 mg-CH₄C m⁻²
 500 d⁻¹ for the eastern thawing wet sector and 2419 mg-CH₄C m⁻² d⁻¹ for the western sector. Detailed
 501 emissions for all years are presented in Table 54. The peak season emissions were statistically
 502 different from each other ($p < 0.001$). Wintertime fluxes were steadily declining as winter
 503 continued and the lowest emissions were observed slightly before the spring thaw. Wintertime
 504 average emissions were 249 mg-CH₄C m⁻² d⁻¹ for the eastern sector and 166 mg-CH₄C m⁻² d⁻¹
 505 for the western sector. Detailed emission emissions of winter periods are presented in Table 65.

506 Table 54. CH₄ emission during the peak season

	Mean	Standard deviation	The standard error of the mean
	[mg-CH ₄ C m ⁻² d ⁻¹]		
2014 E	54.240.7	22.317.2	6.54.3
2015 E	55.334.4	13.211.7	2.83.7
2016 E	59.945.4	9.46.7	21.7
2014 W	2218.6	4.53.2	1.20.8
2015 W	21.416.1	43.2	1.40
2016 W	28.220.9	3.72.6	10.7

507

508 Table 65. CH₄ emission during the winter period

Formatted: Font: (Default) +Body (Calibri), Not Bold, Not Italic

Formatted Table

Formatted: Font: 11 pt, Not Bold, Not Italic

Formatted: Font: 11 pt, Not Bold, Not Italic

Formatted: Font: (Default) +Body (Calibri), Not Bold, Not Italic

Formatted: Font: (Default) +Body (Calibri), Not Bold, Not Italic

Formatted: Font: (Default) +Body (Calibri), Font color: Auto

Formatted: Font: (Default) +Body (Calibri)

Formatted: Font: (Default) +Body (Calibri), Font color: Auto

Formatted: Font: (Default) +Body (Calibri)

Formatted: Font: (Default) +Body (Calibri), Font color: Auto

Formatted: Font: (Default) +Body (Calibri)

Formatted: Font: (Default) +Body (Calibri), Font color: Auto

Formatted: Font: (Default) +Body (Calibri)

Formatted: Font: (Default) +Body (Calibri), Font color: Auto

Formatted: Font: (Default) +Body (Calibri)

Formatted: Font: (Default) +Body (Calibri), Font color: Auto

Formatted: Font: (Default) +Body (Calibri)

	Mean	Standard deviation	The standard error of the mean
	[mg-CH ₄ C m ⁻² d ⁻¹]		
2014 E	24.19.0	5.52.8	0.74
2015 E	228.3	3.51.7	0.42
2016 E	26.39.8	52.6	0.53
2014 W	197.2	52.2	1.10.4
2015 W	14.95.5	2.81.4	0.42
2016 W	14.05.2	3.14	0.4

509

510

511 3.3 Factors controlling the CH₄ fluxes

512 In the eastern sector, the CH₄ flux correlated best with the peat temperature at 30 cm depth, and
 513 in the western sector with the temperature at 10 cm depth. Using temperatures above the level
 514 of maximum correlation led to similar hysteresis-like behavior in CH₄ flux - temperature relations
 515 as presented by Chang et al. (2020), but using deeper temperatures led to inverse hysteresis
 516 compared to shallower temperatures (Figure 56). The correlation matrix (Figure S2S3) shows the
 517 importance of SWC in the CH₄ emissions, while WTL does not correlate significantly with CH₄ flux.
 518 Controlling factors were examined before and after temperature normalization (Table 7), of the
 519 CH₄ fluxes following Rinne et al. (2018) (Table 6), in order to avoid effect of cross-correlation
 520 between explanatory parameters.

521

Formatted: Font: (Default) +Body (Calibri)

Formatted Table

Formatted: Font: (Default) +Body (Calibri), Not Bold, Not Italic

Formatted: Font: (Default) +Body (Calibri), Not Bold, Not Italic

Formatted: Font: 11 pt, Not Bold, Not Italic

Formatted: Font: 11 pt, Not Bold, Not Italic

Formatted: Font: (Default) +Body (Calibri), Not Bold, Not Italic

Formatted: Font: (Default) +Body (Calibri)

Formatted: Font: (Default) +Body (Calibri), Font color: Auto

Formatted: Font: (Default) +Body (Calibri)

Formatted: Font: (Default) +Body (Calibri), Font color: Auto

Formatted: Font: (Default) +Body (Calibri)

Formatted: Font: (Default) +Body (Calibri), Font color: Auto

Formatted: Font: (Default) +Body (Calibri)

Formatted: Font: (Default) +Body (Calibri), Font color: Auto

Formatted: Font: (Default) +Body (Calibri)

Formatted: Font: (Default) +Body (Calibri), Font color: Auto

Formatted: Font: (Default) +Body (Calibri)

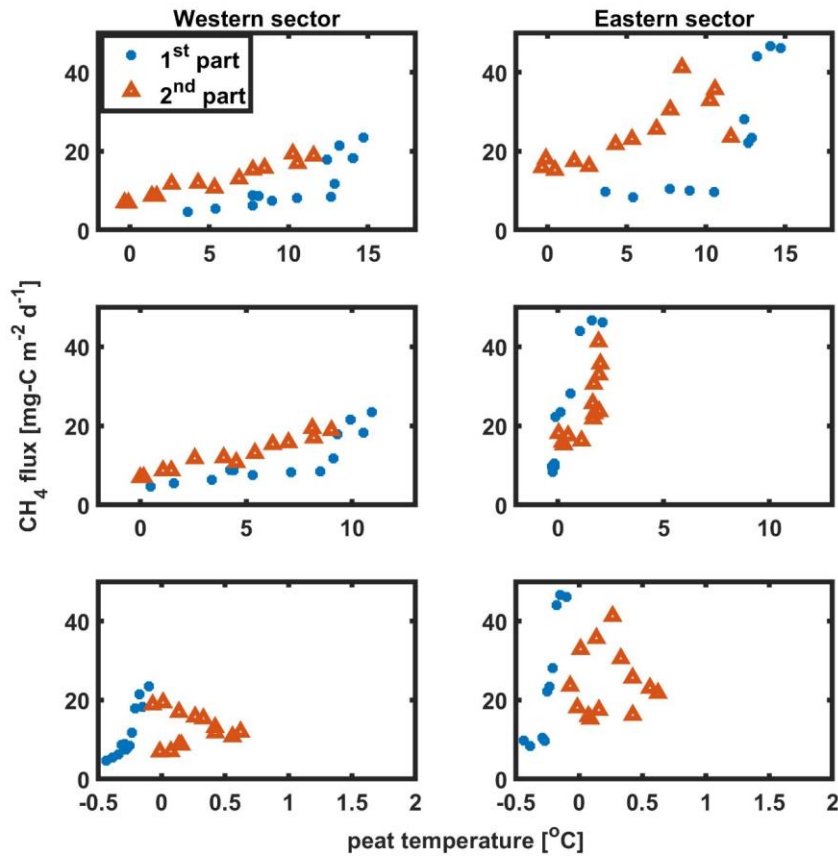
Formatted: Font: (Default) +Body (Calibri), Font color: Auto

Formatted: Font: (Default) +Body (Calibri)

Formatted: Font: +Body (Calibri)

Formatted: Subscript

Formatted: Font: 11.5 pt



522

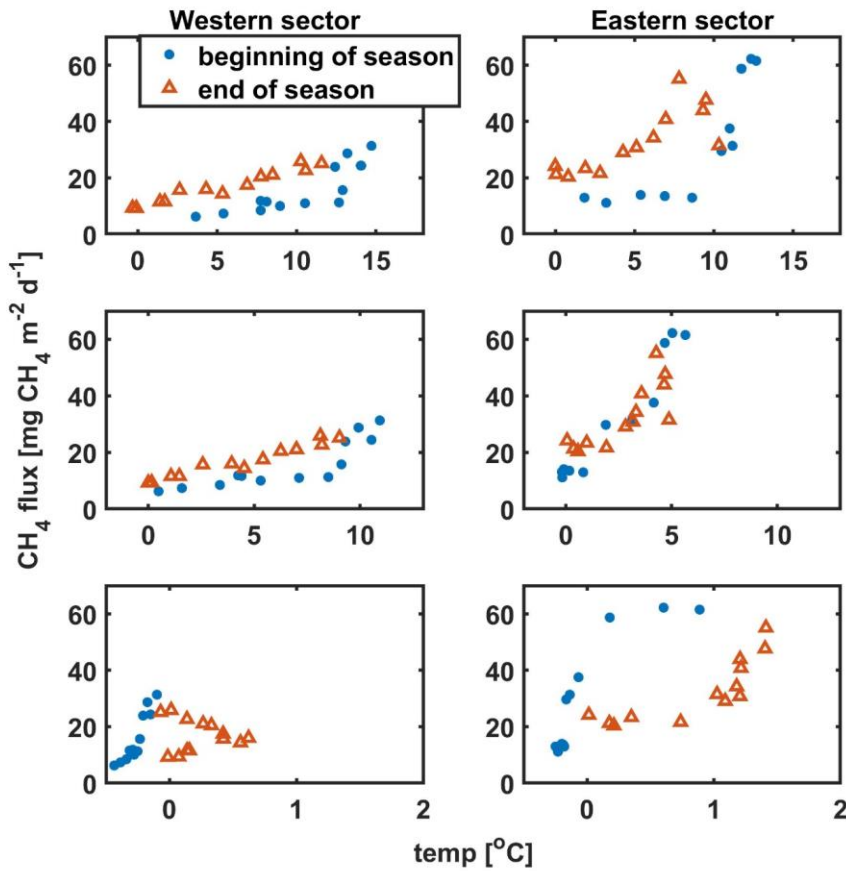
523 Figure 56. Weekly averages of CH₄ fluxes ~~vs~~against the surface peat temperature (top panels), ~~vs~~the
 524 ~~depth with~~ best ~~correlated layer correlation~~ (middle panels), and ~~vs~~the deeper layer (bottom panel). Data
 525 were divided into the ~~beginning~~1st part of the growing season (blue dots) ~~before the maximum weekly~~
 526 ~~emission, and end~~2nd part of the growing season (orange triangles), ~~where breakout week was the week~~
 527 ~~with the highest emission.~~ after that.

Formatted: Font: 11.5 pt

Formatted: Justified

Formatted: Font: 11.5 pt

Formatted: Font: 12 pt



528

529

530 The result from GLM, showing the variables that contribute to the model, is presented in Table
 531 S2. The parameter which that was selected first by all models, was peat temperature, at 10 cm
 532 depth for the western sector and at 30 cm depth for the eastern sector. For the eastern sector,
 533 the GLM algorithm selected SWC as the explanatory factor for CH₄ fluxes during all years as well
 534 as for the combined three-year period. The GLMs created for the western sector did not have
 535 other explanatory factors besides the peat temperature that were selected in all years. However,
 536 two more explanatory factors, GPP and shortwave incoming radiation, appeared in the three
 537 time periods (years 2015 and 2016, and three-years combined) for the western sector.

538 The eastern sector models had shortwave incoming radiation as the explanatory factor for the
 539 year 2015, the year 2016, and combined three-year period. A unique variable for this sector was
 540 the vapor pressure deficit, which was used in the models constructed for the years 2016 and
 541 combined three-year period.

542 The year 2014 ~~for both sectors~~ was characterized by a smaller number of parameters contributing
 543 to the models for both sectors compared to other years and combined three-year models. Only
 544 peat temperature and SWC were explanatory variables for both sectors in this year. The years
 545 2015 and 2016 and all three years combined have a longer list of parameters.

546 As the WTL data was available only during a short period of the year, it was not analyzed with
 547 ~~usage of~~ the GLM. The WTL measurement in the western sector was not representative of the
 548 conditions for most of the sector, this parameter was not used for further analysis from this
 549 sector. The WTL was correlated with CH₄ fluxes for the eastern sector.

550 Based on the chosen explanatory variables it ~~could be was~~ noticed that the seasonal cycle could
 551 be explained by a lower number of parameters than the interannual variation.

552 Table 7-6. Summary of controlling factors before and after temperature normalization

Year and ecosystem	R for CH ₄ flux	the p-value for CH ₄ flux	R for temperature normalized CH ₄ flux	the p-value for temperature normalized CH ₄ flux
GPP				
2014 E	0.71	7x10 ⁻²²	-0.03	0.70
2015 E	0.69	2x10 ⁻²⁵	0.02	0.83
2016 E	0.77	1x10 ⁻³⁶	0.21	4x10 ⁻³
2014 W	0.69	4x10 ⁻¹⁵	-0.10	0.36
2015 W	0.73	6x10 ⁻²⁹	0.05	0.56
2016 W	0.71	5x10 ⁻²⁹	-0.02	0.76
WTL				
2014 E	-0.4850	2x10 ⁻⁴	-6x10⁻³ 1x10⁻²	0.9694
2015 E	-0.4620	0.330	-0.220	0.4817
2016 E	0.5760	4x10 ⁻⁶	-0.3330	0.01
SWC				
2014 E	0.51	2x10 ⁻¹⁰	-0.02	0.79
2015 E	0.51	1x10 ⁻¹²	-0.03	0.66
2016 E	0.69	1x10 ⁻²⁶	0.220	6x10 ⁻³
2014 W	-0.31	2x10 ⁻³	-0.37	2x10 ⁻⁴
2015 W	0.19	0.02	-0.19	0.02
2016 W	0.22	3x10 ⁻³	-0.26	5x10 ⁻⁴

553

554

Formatted: Font: (Default) +Body (Calibri), Not Bold, Not Italic

Formatted Table

Formatted: Font: (Default) +Body (Calibri)

Formatted: Font: (Default) +Body (Calibri)

Formatted: Font: (Default) +Body (Calibri)

Formatted: Font: (Default) +Body (Calibri)

Formatted: Font: (Default) +Body (Calibri)

Formatted: Font: (Default) +Body (Calibri)

Formatted: Font: (Default) +Body (Calibri)

Formatted: Font: (Default) +Body (Calibri)

Formatted

Formatted

Formatted

Formatted: Font: (Default) +Body (Calibri)

Formatted

Formatted

Formatted

Formatted

Formatted

Formatted

Formatted

Formatted

Formatted

Formatted

Formatted

Formatted: Font: (Default) +Body (Calibri)

Formatted: Font: (Default) +Body (Calibri)

Formatted: Font: (Default) +Body (Calibri)

Formatted: Font: (Default) +Body (Calibri)

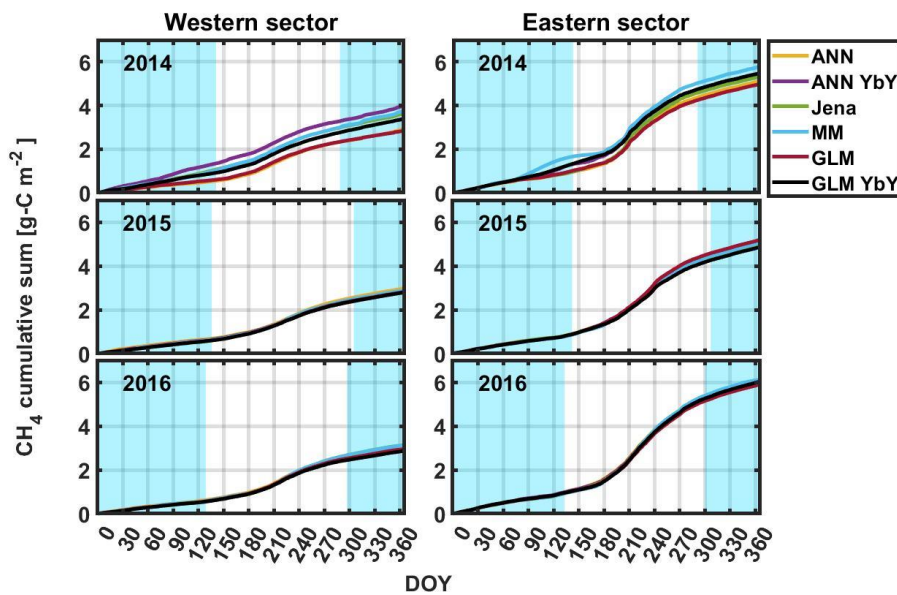
Formatted: Font: (Default) +Body (Calibri)

Formatted: Font: (Default) +Body (Calibri)

555 **3.4 Gap-filled annual cycles**

556 Cumulative CH₄ emissions based on different gap-filling methods are presented in Figure 67. All
557 follow a similar annual curve, with a steeper increase in summer, but also relatively high
558 wintertime contribution. Annual, wintertime, and unfrozen period emissions by all gap-filling
559 methods, with their estimated uncertainties, are shown in Figure 78. Emission estimation by each
560 sector and data gap-filled by the different method are presented in Table S3. Average values from
561 all models with their upper and lower limit and wintertime contribution to fluxes are
562 demonstrated in Table 87.

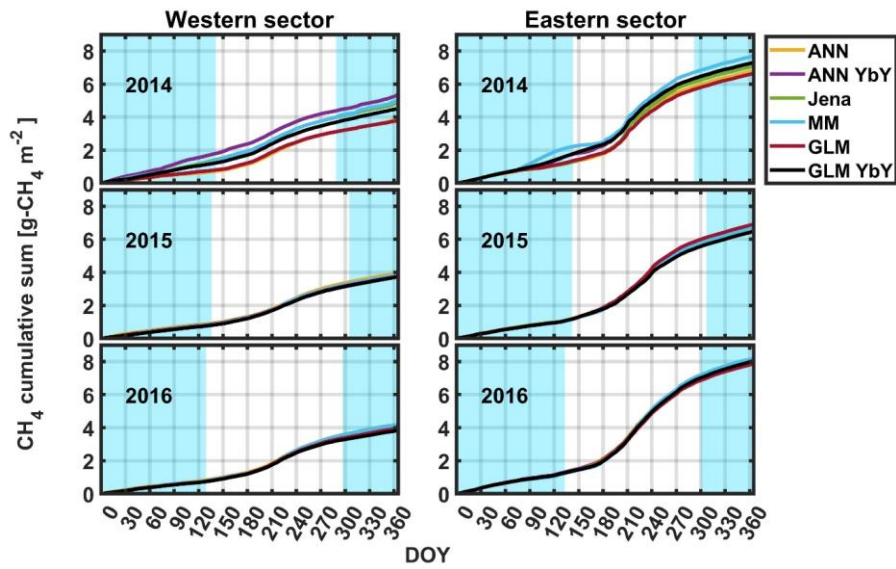
Formatted: Font: (Default) +Body (Calibri)



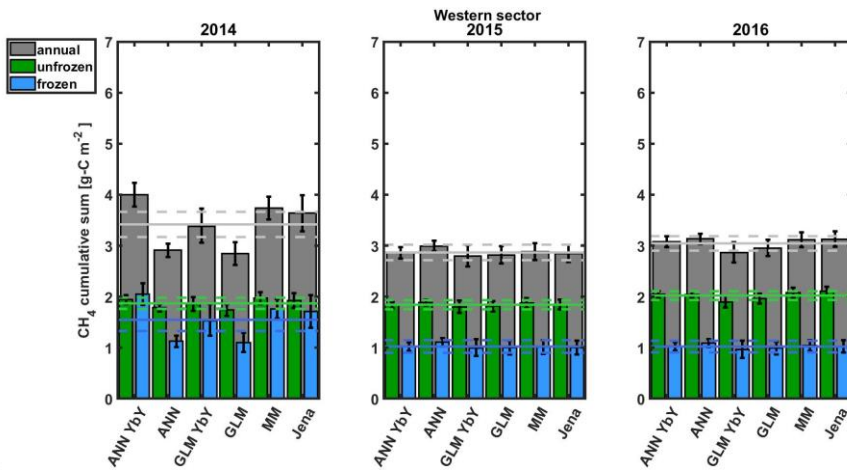
Formatted: Line spacing: Multiple 1.08 li

563
564 Figure 67. The cumulative sum of CH₄ fluxes for the years 2014-2016 for western and eastern sectors
565 calculated with the different gap-filling methods. ANN - the artificial neural network for all years, ANN
566 YbY - artificial neural network each year separately, Jena - Jena online gap-filling tool, MM - moving
567 mean with 5-day moving window, GLM- the general linear model for all years, GLM YbY - the general
568 linear model for each year separately. The shaded light blue area is designated the frozen period when
569 peat temperature at 10 cm was below 0°C (see chapterSection 2.8 for a detailed description).

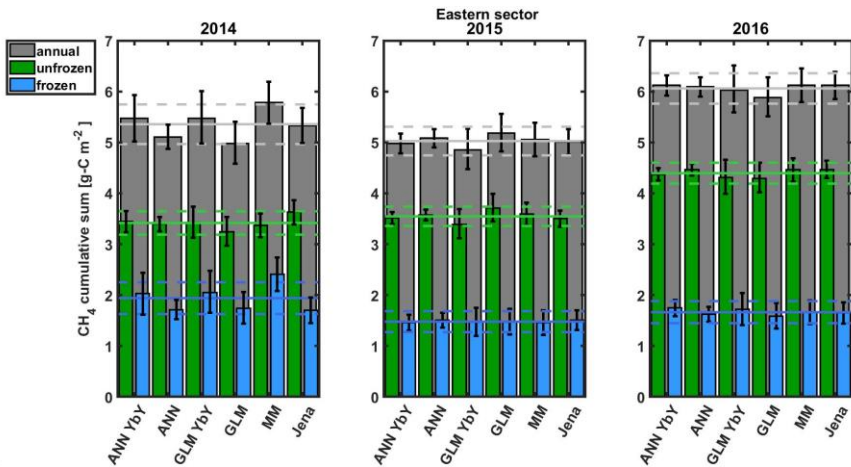
Formatted: Font: (Default) +Body (Calibri)



570
571
572

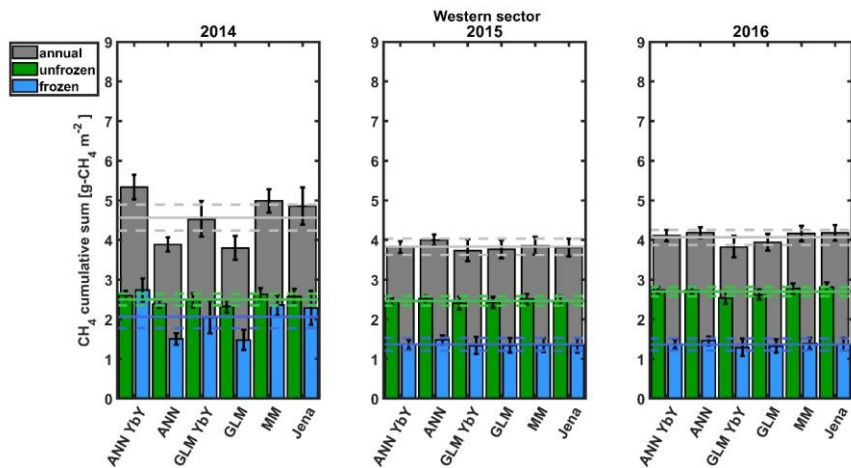


573

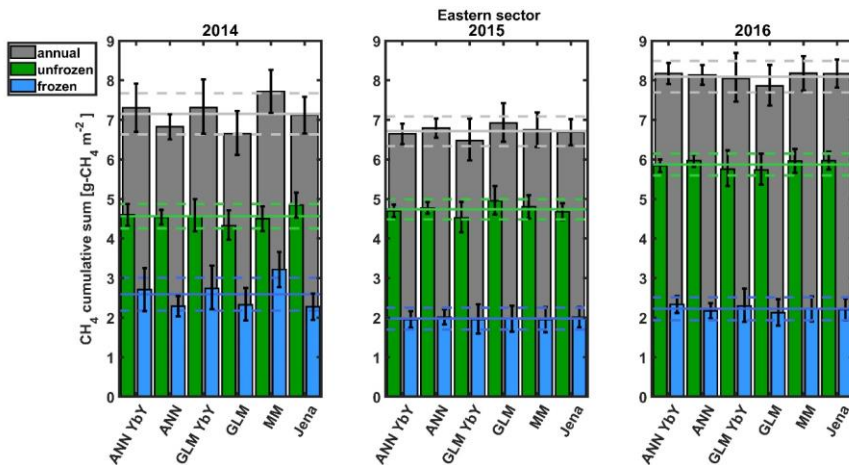


574

575 Figure 78. Comparison of cumulative sums of CH₄ fluxes for different gap-filling methods for the western
 576 sector (top panel) and eastern sector (bottom panel). ANN - the artificial neural network for all years, ANN
 577 YbY - artificial neural network each year separately, Jena - Jena online gap-filling tool, MM - moving mean
 578 with 5-day moving window, GLM- the general linear model for all years, GLM YbY - the general linear
 579 model for each year separately. Gray bars are for the annual sums, blue bars are for the frozen period
 580 sums and green bars are for the unfrozen period (see [chapterSection 2.8 for a detailed description](#)). Solid
 581 lines are the mean value from all models and dashed lines are for the standard deviation range, with the
 582 same colors described above.



583



584
585

586 As can be seen in Table 43, the year 2014, with a larger difference between annual emissions
587 calculated by different gap-filling methods, had very long gaps that were not present in other
588 years. Also, the uncertainties in annual emission are the largest for the year 2014 for all gap-filling
589 methods, reflecting the gap distribution.

590

591 Table 87. Average CH₄ annual annual emission based on all models with the upper and lower
592 limit and contribution to from the wintertime fluxes.

	Western sector			Contribution to wintertime fluxes (%)	Eastern sector			Contribution to wintertime fluxes (%)
	Mean	Lower limit	Upper limit		Mean	Lower limit	Upper limit	
	g-CH ₄ C m ⁻² yfa ⁻¹				g-CH ₄ C m ⁻² yfa ⁻¹			
2014	3.4.6	32.8	5.34.0	45	7.25.4	6.75.0	7.75.8	36
2015	32.8	3.72.8	43.0	36	6.75.0	6.54.9	6.95.2	29
2016	43.1	32.8	4.23.1	34	86.1	75.9	8.26.1	27

593

594 Three years' averages of GPP and net ecosystem exchange (NEE) for two sectors are presented
595 in table 98. As a comparison, data from a lake and tall sedge fen areas at the Stodalen mire
596 complex, where permafrost was completely thawed, of Stodalen Mire by are also presented
597 (Jammet et al. (., 2017) are presented, showing that the). The fen has the highest percentage of
598 carbon emitted as CH₄, as compared to the annual CO₂ uptake. The eastern and the western

Formatted: Font: (Default) +Body (Calibri), Not Bold, Not Italic

Formatted: Font: (Default) +Body (Calibri)

Formatted: Font: (Default) +Body (Calibri), Not Bold, Not Italic

Formatted: Font: (Default) +Body (Calibri)

Formatted: Font: (Default) +Body (Calibri), Not Bold, Not Italic

Formatted: Font: (Default) +Body (Calibri)

Formatted: Font: (Default) +Body (Calibri), Not Bold, Not Italic

Formatted: Font: (Default) +Body (Calibri)

Formatted: Font: (Default) +Body (Calibri), Not Bold, Not Italic

Formatted: Font: (Default) +Body (Calibri)

Formatted: Font: (Default) +Body (Calibri), Not Bold, Not Italic

Formatted: Font: (Default) +Body (Calibri)

Formatted: Font: (Default) +Body (Calibri), Not Bold, Not Italic

Formatted: Font: (Default) +Body (Calibri)

Formatted: Font: (Default) +Body (Calibri)

Formatted: Font: (Default) +Body (Calibri)

Formatted: Font: (Default) +Body (Calibri)

Formatted: Not Strikethrough

sectors emitted less of the assimilated carbon as CH₄ compared to the completely thawed area. The uptake of carbon as CO₂ was also largest at the fen.

Table 98. Average annual GPP, NEE and CH₄ emission from western and eastern sector in comparison to fen.

	GPP	NEE	CH ₄	CH ₄ /GPP	CH ₄ /NEE
	g-C m ⁻² a ⁻¹	g-C m ⁻² a ⁻¹	g-C m ⁻² a ⁻¹	%	%
Western sector	225	-28.9	3.1	1.4	19.6
Eastern Sector	257	-42.0	5.5	2.2	14.0
Fen (Jammet et al. 2017)	N.A.	-66.3	21.2	N.A.	32.0

The 3 years' annual average annual CH₄ emissions of palsa and thawing surfaces, as calculated by Eqs. (1) and (2), are presented in Table 109. For comparison average annual emissions from other major surface types, measured by EC technique, are shown as well. The emission from the tall graminoid fen, a third mire type common at Stordalen Mire, has been previously measured using the EC method by Jackowicz-Korczyński et al. (2010) and Jammet et al. (2017). In addition to these, the mire complex includes shallow lakes. Their annual CH₄ emission has been measured by EC method by Jammet et al., (2017).

Table 109. Annual CH₄ emission from different components of the Stordalen Mire complex from EC studies.

type of wetland	Annual emission [g-CH ₄ -C m ⁻² y ⁻¹]	References
palsa plateau surface	3.62.7 ± 0.75	this study
thawing wet surface	11 ± 8.2 ± 1.5	this study
thawed fen	21.15.8 ± 1 ± 2.2.6	Jackowicz-Korczyński et al. 2010
thawed fen	28.321.2 ± 1.73	Jammet et al. 2017
shallow lake	6.54.9 ± 0.86	Jammet et al. 2017

4 Discussion

4.1 Differences in controlling factors

According to the GLM, peat temperature and GPP were typically the first parameters selected by the algorithm to explain CH₄ fluxes. In the eastern sector, the CH₄ flux correlated best with the peat temperature at 30 cm depth, and in the western sector with the peat temperature at 10 cm depth. Temperature as a controlling factor of CH₄ emission has been reported in many wetlands studies (Christensen et al. 2003, Jackowicz-Korczyński et al. 2010, Bansal et al. 2016, Pugh et al. 2017, Rinne et al. 2007; 2018), in line with our findings. The correlation of CH₄ fluxes with the

622 temperature at 5 cm depth was also higher than for 30 cm in the western sector. As the peat in
623 the palsa is frozen at 30 cm depth for most of the growing season, the correlation between CH₄
624 fluxes and temperature at these depths is lower. Temperature correlation for the upper part,
625 2 cm, and 5 cm depth, shows a similar level of correlation as presented by Jackowicz-Korczyński
626 et al. (2010). As they did not analyze correlation with the temperature at deeper peat, we cannot
627 compare these results. The hysteresis-like behavior of the CH₄ flux – temperature relation is
628 similar to that observed by Chang et al. (2020) when using temperatures measured above the
629 depth of maximum correlation, but inversed when using temperatures measured at deeper
630 depths (Figure 56). This is in line with at least part of the hysteresis-like behavior to be due to the
631 lag of seasonal temperature wave at the depth of methane CH₄ production compared to the
632 timing of the temperature wave at shallower depth or air temperature.

633 GPP was indicated as a controlling factor for CH₄ emission from a boreal fen ecosystem by Rinne
634 et al. (2018). In our study, the correlation matrix shows a significant correlation between daily
635 average GPP and CH₄ flux at both sectors (Table S3). To disentangle the confounding effects of
636 temperature and GPP, we used temperature-normalized CH₄ fluxes following Rinne et al. (2018)
637 which revealed that the correlation between GPP and temperature-normalized CH₄ flux was not
638 significant in most years (Table 7-6). Only the data from the eastern sector in the year 2016
639 shows a significant correlation. Thus, it seems hard to disentangle the effects of temperature and
640 GPP on CH₄ fluxes using this data set. As our data set consists of only three years, the analysis of
641 interannual variations would not be a robust approach either.

642 Solar shortwave incoming radiation was selected as a controlling variable by 6 of 8 GLM models
643 (Table S3). This parameter has an indirect effect on CH₄ production via photosynthesis and
644 subsequent substrate production. The maximum emission of CH₄ occurs later in the year than
645 maximum radiation. This may be due to the CH₄ emission depending on the deeper peat
646 temperature or seasonal cycle of available substrates, lagging behind the annual cycle of
647 radiation (e.g. Rinne et al., 2018; Chang et al., 2020). The negative contribution of shortwave
648 radiation in GLM can be due to the slight diel cycle of CH₄ emission, with lowest values at
649 daytime. Mechanistically we can think that the solar irradiance will heat the top of the peat layer,
650 thus leading to increased methanotrophy at daytime (see discussion above on diel cycle). This
651 can lead to situation where the methanotrophy is higher in sunny days with warm surface and
652 lower in cloudy days. The role of photosynthesis for the substrate supply of methanogenesis is
653 likely to act in the seasonal time scale, where its effect can be masked by the strong correlation
654 between peat temperature and CH₄ emission. The highest correlation of CH₄ flux and radiation
655 was observed in 2014, but GLM did not select radiation as an explanatory factor for this year.
656 Other years and the whole period show a much lower correlation.

657 CH₄ fluxes from wetlands have been shown to depend on WTL in many studies (e.g. Bubier et al.,
658 2005; Turetsky et al., 2014; Rinne et al., 2020). However, in a number of studies, the CH₄ fluxes
659 have shown to be relatively insensitive to the small variation, without strong extreme conditions,
660 in the WTL (Rinne et al. 2007, 2018, Jackowicz-Korczyński et al. 2010). In the eastern sector, CH₄
661 flux and WTL were correlated for the years 2014 and 2016. However, after normalization of CH₄
662 fluxes with their temperature dependence following Rinne et al., (2007), correlations were

Formatted: Font: (Default) +Body (Calibri)

Formatted: Default

663 mostly not significant (Table 76). This is similar to conclusions drawn by e.g. Rinne et al. (2007,
664 2018) and Jackowicz-Korczyński et al. (2010).

665 Instead of WTL, we used SWC as a possible controlling factor for the CH₄ emission from the
666 western sector. Sturtevant et al. (2012) also reported SWC as a controlling factor in autumn. SWC
667 shows correlation on a significant level before and after normalization for three years for the
668 western sectors (Table 76).

669 The GLM algorithm selected SWC as one of the explaining factors while constructing the GLM for
670 the eastern sector for the whole measurement season. It was chosen by models built for three
671 years together and each year separately. R and p-value are presented in Table 76. A reduction of
672 R and increase in p-value after temperature normalization is similar to previous parameters. The
673 correlation of CH₄ emission with SWC stays on a significant level only in the year 2016.

674

675 4.2 Gap-filling methods

676 In general, the gap-filled annual CH₄ emissions were within their estimated uncertainty from each
677 other, apart from the year 2014. The results of different gap-filling methods were affected by the
678 different gap distributions and lengths in different years and the two wind sectors. Thus, below
679 we discuss the method performance separately for the year 2014 and the two other years.

680 The dataset from the eastern sector was gap-filled with ~~less uncertainty~~ **higher confidence** than
681 for the western sector in 2014. The data from the eastern sector contains fewer very long gaps -
682 more than 30 days, and fewer long gaps - more than 8 but less than 30 days. The method which
683 was most affected by long gaps was the moving mean approach, indicating that this method
684 should not be used for data sets with very long gaps. The ANN and the GLM gap-filling methods
685 based on the whole data set estimated lower annual emission than mean emission from all
686 methods. For two years without very long gaps (2015 and 2016), the Jena gap-filling tool was
687 assumed as a baseline method, as it is commonly used for gap-filling of especially CO₂ fluxes. It
688 is independent of the user choices, as the ecosystem variables required have been chosen by the
689 developers. However, as this gap-filling tool has been developed ~~with~~ **for** CO₂ ~~in mind~~, not all the
690 variables are necessarily relevant for the gap-filling of the CH₄ time series. Furthermore, the Jena
691 gap-filling tool works in a half-hourly resolution to resolve the diel variation in CO₂ fluxes. As the
692 sub-daily variation in CH₄ fluxes is largely random noise in many mires (Rinne et al., 2007; 2018;
693 Jackowicz-Korczyński et al., 2010), developing a similar tool working at daily time step for CH₄,
694 and with tailored parameter set for ~~methane~~ **CH₄**, would be useful.

695 The moving mean approach resulted in annual fluxes within the range of standard deviation from
696 the Jena gap-filling tool. Daily values ~~could~~ **probably** vary less than values obtained by the Jena
697 tool because moving means smooth the data. Additional advantages of this method are low **input**
698 requirements, as no auxiliary data is needed.

Formatted: Font: (Default) +Body (Calibri)

699 Annual estimates of CH₄ emission, based on the gap-filling with algorithms developed for the
700 whole data set, could be biased when the ecosystem is changing fast between the years and
701 functional dependencies on environmental parameters change. The annual CH₄ emissions by
702 ANN, based on the whole data set and based on one-year data, agree within the standard
703 deviation for the years 2015 and 2016. Both of them are ~~als~~ also in agreement with the
704 baseline method within the standard deviation.

705 The feasibility of GLM is similar to ANN. The GLM model built on the whole dataset is sensitive to
706 rapid changes in ecosystem functioning and the number of gaps each year. A year with more gaps
707 has a lower influence on the model, similarly to the ANN. However, annual CH₄ emissions derived
708 using GLMs, based on each year separately or the whole dataset, agree with one another and
709 with baseline model within the standard deviation. GLM required more preparation than ANN.
710 Before developing the GLMs, highly correlated parameters need to be determined. The selection
711 of relevant variables is crucial for the correct performance of that algorithm and the selection
712 influences model output and model uncertainties.

713 According to the analysis with artificial gaps, the 35-day artificial gap did not change annual sums
714 significantly for any gap-filling method. The 80-day artificial gap created a significant difference
715 for the eastern sector in the year 2015 for ANN YbY and 2016 for ANN- (Figure ~~S5-S7~~). The
716 unfrozen period did not show significant differences between annual sums for any method. The
717 wintertime period was statistically different for the year 2015 for ANN YbY. The results with the
718 80-day gap had higher uncertainties than the results with a 35-day gap. The existence of gaps in
719 the winter period did not have a significant impact on the unfrozen period fluxes.

720 All presented methods show similar CH₄ emissions. Choosing one of them as the most
721 appropriate is not obvious, because all of them ~~has strong~~ show both advantages and ~~week~~
722 ~~points. Method~~ disadvantages. The method that required the ~~less~~ least amount of preparation
723 before use, ~~so and that was thus~~ the ~~faster~~ fastest to apply is ~~the~~ moving mean. It can be used for
724 ~~the~~ short gaps with ~~the~~ good results and does not need additional measured variables to work
725 properly. The ANN method require less preparation than other methods i.e. following the
726 template or choosing the correct variables and it gives similar results. It could be recommended
727 as a gap-filling method suitable for different sites due to unique construction of the ANN for each
728 place.

729

730 4.3 Winter fluxes

731 The winter fluxes from both sectors were positive, which is in line with observations by e.g. Rinne
732 et al. (2007, 2018, 2020) and Jammet et al. (2017) of wintertime CH₄ emissions from frozen
733 northern mires. Winter emission and potential spring thaw bursts of CH₄ can be mechanistically
734 connected (Taylor et al. 2018), while degassing of CH₄ during the winter is likely to lead to smaller
735 or no thaw bursts of CH₄. Thus, EC studies on the seasonal cycle of CH₄ emissions from other
736 seasonally frozen mire ecosystems have shown minor or no thaw emission pulse (Rinne et al.,

Formatted: Subscript

Formatted: Font: (Default) +Body (Calibri)

737 2007; 2018; Mikhaylov et al. 2015). On the contrary, many studies show spring-thaw emissions
738 from shallow lakes (Raz-Yaseef et al. 2017, Jammet et al. 2015, 2017). In lakes, winter fluxes can
739 be blocked by a solid ice layer leading to the build-up of CH₄ below ice during the frozen period
740 (Jammet et al. 2017). On mires, however, the ice cover is not as solid as in lakes, but more porous
741 due to peat and plants within the ice. Therefore, the diffusion during the frozen period is
742 considerably faster than through lake ice. Furthermore, Song et al. (2012) showed that spring
743 burst events could occur at a very small scale and very short in duration (e.g. 2 hours). Small-scale
744 events show a lower influence on EC measurements because the method averages over a larger
745 area. Moreover, if the small-scale short-duration event does not happen in the EC footprint e.g.
746 due to wind direction, it will be missed.

747 We did not observe an autumn freeze-in burst in our data from either sector at Stordalen Mire.
748 These events have been observed at a High-Arctic tundra site (Mastepanov et al. 2013) though
749 not every year. Mastepanov et al. (2008) suggested that freeze-in bursts of CH₄ could be observed
750 only in the Arctic with continuous permafrost and not in a subarctic area with discontinuous or
751 sporadic permafrost. The phenomenon is assumed to be connected to the expansion of water
752 upon freezing, causing air bubbles to be mechanically pushed out of the freezing soil.

753

754 4.4 Different permafrost status and CH₄ emissions

755 Stordalen Mire is a complex mire system, with at least three different main wetlands surface
756 types and different permafrost ~~statuses~~status within a distance of a few hundred meters. The
757 permafrost palsa development and thaw depend both on temperature and snow cover and it is
758 partly self-regulating via the effect of microtopography on local snow depth (Johansson et al.
759 2006). Due to the recently increasing temperatures, the thaw processes are currently likely to
760 dominate over palsa growth. CH₄ emission from the different microforms in mire systems
761 depends on ~~at~~the hydrological and nutrient status and temperature which affect e.g. plant and
762 microbial communities.

763 The carbon emitted as the CH₄ fluxes from the eastern and western sector is on similar level to
764 the Siikaneva fen (Rinne et al. 2018). In comparison to the other ~~fens~~fen sites reviewed by Rinne
765 et al. (2018;), ~~the~~ the ratio of CH₄ to NEE at Stordalen Mire is higher. The reason behind this could be
766 ~~the~~ shorter growing season and thus lower CO₂ fluxes.

767 The average annual CH₄ emissions from different surfaces (Table 109) shows that the palsas have
768 the lowest annual CH₄ ~~emission~~emissions, followed by a lake. The fully thawed fen, dominated
769 by tall graminoids, has very high annual CH₄ ~~emission~~emissions and the highest of the mire
770 complex, surpassing e.g. many boreal poor fens (Nilsson et al., 2008; Rinne et al., 2018). The
771 thawing surfaces common in the eastern footprint ~~of the tower~~ have annual CH₄
772 ~~emission~~emissions between palsas and tall sedge fen. The three surface types studied here and
773 previously by Jackowicz-Korczyński et al. (2010) and Jammet et al., (2017) can be seen as forming

Formatted: Font: (Default) +Body (Calibri)

Formatted: Subscript

Formatted: Font: (Default) +Body (Calibri)

774 a thaw gradient in this subarctic environment. The globally rising temperature is likely to lead to
775 continuing permafrost thaw in this kind of ~~system~~ecosystem and increased CH₄ emissions.

776

777 5 Conclusion

778 At our study site, eddy covariance fluxes were measured for two different subarctic mire areas,
779 one dominated by palsa plateaus and the other a mixture of palsas and thawing wet surfaces.
780 The measurements revealed clear differences in their annual CH₄ ~~emission~~emissions, with the
781 area dominated by palsas emitting less. The annual emission from a thawing surface (118.2 g-
782 CH₄C m⁻² da⁻¹) was nearly three times higher than from palsa surfaces (3.62.7 g-CH₄C m⁻² da⁻¹) but
783 only half of the emission previously reported from fully thawed tall graminoid fen. Areas
784 measured in this study had similar seasonal cycles of emission, with maxima appearing in August
785 and lower but significant fluxes in winter. The seasonal cycles were furthermore characterized by
786 a gentle~~fast~~ increase in spring (average 0.21 mg-C m⁻² d⁻² for the western sector and 0.68 mg-C
787 m⁻² d⁻² for the eastern sector) and a more~~less~~ rapid decrease in fall, (average -0.16 mg-C m⁻² d⁻²
788 for the western sector and -0.37 mg-C m⁻² d⁻² for the eastern sector), without any obvious burst
789 events during spring thaw or autumn freeze-in. The wintertime period (from January to mid-May
790 and from late-October to December) contributed with 27-% - 45 % to the annual emission.

791 According to the correlation matrix and GLM analysis, CH₄ emissions from the western and
792 eastern sectors were partly controlled by different factors. As in most studies on CH₄ emission
793 from wetlands, peat temperature was the most important factor explaining the emission.
794 ~~However, the temperature at different depths seemed to control the CH₄ fluxes for the two~~
795 ~~analyzed mire sectors.~~The relation of CH₄ flux with peat temperature at shallower depths
796 showed similar hysteresis-like behavior than observed by Chang et al. (2020), but inverse
797 behavior with temperature at deeper peat. We showed that the existence and direction of
798 hysteresis-like behavior can depend on which depth the temperature is measured.

799 The correlation of CH₄ emission and WTL in the eastern sector was not significant, but in the
800 western sector, the SWC did appear to control the emission.

801 The estimation of annual CH₄ emission was based on gap-filling with four different methods. All
802 methods resulted in ~~rather~~ similar annual fluxes, especially for the two years with just relatively
803 short gaps- (less than 8 days). The performance of the methods was also dependent on atthe gap
804 distribution. ~~The longer~~Long gaps (more than 8 days) were the most problematic to be
805 reconstructed by any of the methods. The average annual emission from the western sector was
806 4.23.1 g-CH₄C m⁻² yr⁻¹ and from the eastern sector was 7.35.5 g-CH₄C m⁻² yr⁻¹. Both were
807 substantially lower than those obtained from a tall graminoid fen at the same mire system.

808 Based on the presented results further studies should focus on winter fluxes, which are important
809 in the northern, low emissions wetlands with discontinuous permafrost. There is still a lack in
810 understanding ~~of~~ the processes behind those emissions. Also, the origin of wintertime CH₄

Formatted: Font: (Default) +Body (Calibri)

Formatted: Font: (Default) +Body (Calibri)

Formatted: Font: 11 pt, Font color: Black

Formatted: Font: (Default) +Body (Calibri)

811 emission is somewhat unknown. On the one hand, CH₄ can be produced during the winter period,
812 on the other hand CH₄ can also be produced during the growing season, remain stored in the
813 peat and then be slowly released during the frozen period. These processes could possibly
814 explain the hysteresis-like behavior of CH₄ emissions.

815

816 Data and code availability

817 <http://doi.org/10.5281/zenodo.4640164s>

818

819 Author contribution

820 P.Ł., J.H. T.F., P.C. and J.R. analysed and interpreted the data. P.Ł., J.H., P.C., J.R. wrote the
821 manuscript. T.F., P.C. and, N.R. designed the measurements. N.K. was responsible for the
822 footprint calculation and its interpretation. P.-O.O. and L.E. were responsible for interpreting
823 UAV data. [A. P. supported with the water table level data.](#)

824

825 Competing interests

826 The authors declare that they have no conflict of interest

827

828 Acknowledgements

829 This study is funded by MEthane goes Mobile: MEasurement and MOdeling (MEMO2) project
830 from the European Union's Horizon 2020 research and innovation programme under the Marie
831 Skłodowska-Curie grant agreement No 722479. Data was provided by the Abisko Scientific
832 Research Station (ANS) and Swedish Infrastructure for Ecosystem Sciences (SITES, co-financed by
833 the Swedish Research Council) hosting the Stordalen site, part of the ICOS-Sweden network
834 which was co-financed by the Swedish Research Council (grant-no. 2015-06020, 2019-00205).
835 Image collection using the UAV was done by Matthias Siewert in collaboration with the SITES
836 Spectral project.

837 References

838 [Aubinet, M., Vesala, T., & Papale, D. \(Eds.\) \(2012\). Eddy covariance—A practical guide to
839 measurement and data analysis. Dordrecht: Springer. 978-94-007-2350-4](#)

840 [Åkerman, H. J. and Johansson, M.: Thawing permafrost and thicker active layers in sub-arctic
841 Sweden, Permafr. Periglac. Process., 19, 279–292, <https://doi.org/10.1002/ppp.626>, 2008.](#)

842 [Bansal, S., Tangen, B., and Finocchiaro, R.: Temperature and Hydrology Affect Methane
843 Emissions from Prairie Pothole Wetlands, 36, 371–381, <https://doi.org/10.1007/s13157-016->](#)

Formatted: English (United States)

Formatted: English (United States)

Formatted: Font: (Default) +Body (Calibri)

Field Code Changed

Formatted: Font: (Default) +Body (Calibri)

882 permafrost thaw on C fluxes based on multiyear modeling across a permafrost thaw gradient at
883 Stordalen, Sweden. *Biogeosciences*, 11(17), 4753–4770. <https://doi.org/10.5194/bg-11-4753->
884 2014, 2014.

885 Dengel, S., Zona, D., Sachs, T., Aurela, M., Jammet, M., Parmentier, F. J. W., ~~and~~ Oechel, W., and
886 Vesala, T. (2013).: Testing the applicability of neural networks as a gap-filling method using CH4
887 flux data from high latitude wetlands. *Biogeosciences*, 10(12), 8185–8200.
888 <https://doi.org/10.5194/bg-10-8185-2013>, 2013.

889 Dlugokencky, E. J., Nisbet, E. G., Fisher, R., ~~&and~~ Lowry, D. (2011).: Global atmospheric
890 methane: budget, changes and dangers. *Philosophical Transactions of the Royal Society, Philos.*
891 *Trans. R. Soc. A: Mathematical, Physical and Engineering Sciences*, Math. Phys. Eng. Sci.,
892 369(1943), 2058–2072. <https://doi.org/10.1098/rsta.2010.0341>, 2011.

893 Dobson 1945-, A. J. (2002).: An introduction to generalized linear models / Annette J. Dobson.
894 Boca Raton; Chapman & Hall/CRC, Boca Raton, 2002.

895 Dragomir, C. M., Klaassen, W., Voiculescu, M., Georgescu, L. P., and van der Laan, S.: Estimating
896 Annual CO2 Flux for Lutjewad Station Using Three Different Gap-Filling Techniques, Sci. World
897 J., 2012, 842893, <https://doi.org/10.1100/2012/842893>, 2012.

898 Edie, R., Robertson, A. M., Field, R. A., Soltis, J., Snare, D. A., Zimmerle, D., Bell, C. S., Vaughn, T.
899 L., and Murphy, S. M.: Constraining the Accuracy of Flux Estimates Using OTM 33A, 2019, 1–27,
900 <https://doi.org/10.5194/amt-2019-306>, 2019.

901 Falge, E., Baldocchi, D., Olson, R., Anthoni, P., Aubinet, M., Bernhofer, C., ~~and~~ Burba, G.,
902 Ceulemans, R., Clement, R., Dolman, H., Granier, A., Gross, P., Grünwald, T., Hollinger, D.,
903 Jensen, N.-O., Katul, G., Keronen, P., Kowalski, A., Lai, C. T., Law, B. E., Meyers, T., Moncrieff, J.,
904 Moors, E., Munger, J. W., Pilegaard, K., Rannik, Ü., Rebmann, C., Suyker, A., Tenhunen, J., Tu, K.,
905 Verma, S., Vesala, T., Wilson, K., and Wofsy, S. (2001).: Gap filling strategies for defensible
906 annual sums of net ecosystem exchange. *Agricultural and Forest Meteorology*, *Agric. For.*
907 *Meteorol.*, 107(1), 43–69. [https://doi.org/10.1016/S0168-1923\(00\)00225-2](https://doi.org/10.1016/S0168-1923(00)00225-2), 2001a.

908 Falge, E., Baldocchi, D., Olson, R., Anthoni, P., Aubinet, M., Bernhofer, C., Burba, G., Ceulemans,
909 R., Clement, R., Dolman, H. (A. J.), Granier, A., Gross, P., Grünwald, T., Hollinger, D., Jensen, N.
910 O., Katul, G., Keronen, P., Kowalski, A., Lai, C.-T., and Tu, K.: Gap filling strategies for long term
911 energy flux data sets, Agric. For. Meteorol. 107 71-77, 2001b.

912 Fisher, R. E., France, J. L., Lowry, D., Lanoisellé, M., Brownlow, R., Pyle, J. A., Cain, M., Warwick,
913 N., Skiba, U. M., Drewer, J., Dinsmore, K. J., Leeson, S. R., Bauguutte, S. J.-B., Wellpott, A.,
914 O’Shea, S. J., Allen, G., Gallagher, M. W., Pitt, J., Percival, C. J., Bower, K., George, C., Hayman, G.
915 D., Aalto, T., Lohila, A., Aurela, M., Laurila, T., Crill, P. M., McCalley, C. K., and Nisbet, E. G.:
916 Measurement of the 13C isotopic signature of methane emissions from northern European
917 wetlands, Global Biogeochem. Cycles, 31, 605–623, <https://doi.org/10.1002/2016GB005504>,
918 2017.

919 Friborg, T., Christensen, T. R., and Søgaard, H.: Rapid response of greenhouse gas emission to
920 early spring thaw in a subarctic mire as shown by micrometeorological techniques, Geophys.

Formatted: Font: (Default) +Body (Calibri), English (United States)

Formatted: Font: (Default) +Body (Calibri), Not Italic, English (United States)

Formatted: Font: (Default) +Body (Calibri)

Formatted: Font: (Default) +Body (Calibri), English (United States)

Formatted: Font: (Default) +Body (Calibri)

Formatted: Font: (Default) +Body (Calibri), English (United States)

Formatted: Font: (Default) +Body (Calibri)

Formatted: Font: (Default) +Body (Calibri), English (United States)

Formatted: Font: (Default) +Body (Calibri)

Formatted: Font: (Default) +Body (Calibri), English (United States)

Formatted: Font: (Default) +Body (Calibri)

Formatted: Font: (Default) +Body (Calibri), Not Italic

Formatted: Font: (Default) +Body (Calibri)

Formatted: Font: (Default) +Body (Calibri), Not Italic

Formatted: Font: (Default) +Body (Calibri)

Formatted: Font: (Default) +Body (Calibri), Not Italic

Formatted: Font: (Default) +Body (Calibri)

Formatted: Font: (Default) +Body (Calibri), Not Italic

Formatted: Font: (Default) +Body (Calibri)

Formatted: Indent: Left: 0 cm, First line: 0 cm

Formatted: Font: (Default) +Body (Calibri), Not Italic

Formatted: Font: (Default) +Body (Calibri)

921 [Res. Lett.](https://doi.org/doi:10.1029/97GL03024), 24, 3061–3064, <https://doi.org/doi:10.1029/97GL03024>, 1997.

922 [Gao, X., Adam Schlosser, C., Sokolov, A., Anthony, K. W., Zhuang, Q., and Kicklighter, D.:](#)
 923 [Permafrost degradation and methane: low risk of biogeochemical climate-warming feedback,](#)
 924 [Environ. Res. Lett.](#), 8, 35014, <https://doi.org/10.1088/1748-9326/8/3/035014>, 2013.

925 [Gioli, B., Miglietta, F., Martino, B., Hutjes, R., Dolman, H. \(A. J. ., Lindroth, A., Schumacher, M.,](#)
 926 [Sanz-Sanchez, M.-J., Manca, G., Peressotti, A., and Dumas, E.:](#) [Comparison between tower and](#)
 927 [aircraft-based eddy covariance fluxes in five European regions,](#) [Agric. For. Meteorol.](#), 127, 1–16,
 928 <https://doi.org/10.1016/j.agrformet.2004.08.004>, 2004.

929 Godin, A., McLaughlin, J. W., Webster, K. L., Packalen, M., ~~&and~~ Basiliko, N. ~~(2012).~~: Methane
 930 and methanogen community dynamics across a boreal peatland nutrient gradient. ~~Soil Biology~~
 931 ~~and Biochemistry~~, [Biol. Biochem.](#), 48, 96–105. ~~Soil Biology~~
 932 <https://doi.org/https://doi.org/10.1016/j.soilbio.2012.01.018>, 2012.

933 [Harenda, K., Lamentowicz, M., Samson, M., and Chojnicki, B.:](#) [The Role of Peatlands and Their](#)
 934 [Carbon Storage Function in the Context of Climate Change,](#) in: [GeoPlanet: Earth and Planetary](#)
 935 [Sciences](#), 169–187, https://doi.org/10.1007/978-3-319-71788-3_12, 2018.

936 [Hommeltenberg, J., Schmid, H. P., Drösler, M., and Werle, P.:](#) [Can a bog drained for forestry be](#)
 937 [a stronger carbon sink than a natural bog forest?](#), 11, 3477–3493, [https://doi.org/10.5194/bg-](https://doi.org/10.5194/bg-11-3477-2014)
 938 [11-3477-2014](https://doi.org/10.5194/bg-11-3477-2014), 2014.

939 Intergovernmental Panel on Climate Change (Ed.) ~~(2014).~~: Anthropogenic and Natural
 940 Radiative Forcing. ~~In,~~ in: [Climate Change 2013 – The Physical Science Basis: Working Group I](#)
 941 [Contribution to the Fifth Assessment Report of the Intergovernmental Panel on Climate Change](#)
 942 ~~(pp., Cambridge University Press, Cambridge,~~ 659–740). ~~https://doi.org/DOI:~~
 943 [10.1017/CBO9781107415324.018](https://doi.org/10.1017/CBO9781107415324.018), 2014.

944 [Ise, T., Dunn, A. L., Wofsy, S. C., and Moorcroft, P. R.:](#) [High sensitivity of peat decomposition to](#)
 945 [climate change through water-table feedback,](#) [Nat. Geosci.](#), 1, 763–766,
 946 <https://doi.org/10.1038/ngeo331>, 2008.

947 [Jackowicz-Korczyński, M., Christensen, T. R., Bäckstrand, K., Crill, P., Friborg, T., Mastepanov,](#)
 948 [M., &and Ström, L. \(2010\).: Annual cycle of methane emission from a subarctic peatland.
 949 ~~Journal of Geophysical Research;~~ \[J. Geophys. Res., \\[Biogeosciences\\]\\(#\\), 115\\(G2\\).
 950 <https://doi.org/10.1029/2008JG000913>, 2010.\]\(#\)](#)

951 [Jammet, M., Dengel, S., Kettner, E., Parmentier, F.-J. W., Wik, M., Crill, P., & Friborg, T. \(2017\).](#)
 952 [Year-round CH4 and CO2 flux dynamics in two contrasting freshwater ecosystems of the](#)
 953 [subarctic.](#) [Biogeosciences](#), 14(22), 5189–5216. <https://doi.org/10.5194/bg-14-5189-2017>

954 [Jammet, M., Crill, P., Dengel, S., & Friborg, T. \(2015\).](#) [Jammet, M., Crill, P., Dengel, S., and](#)
 955 [Friborg, T.:](#) Large methane emissions from a subarctic lake during spring thaw: Mechanisms and
 956 landscape significance. ~~Journal of Geophysical Research;~~ [J. Geophys. Res., \[Biogeosciences\]\(#\),
 957 \[120\\(11\\),\]\(https://doi.org/10.1002/2015JG003137\) 2289–2305. <https://doi.org/10.1002/2015JG003137>, 2015.](#)

958 [Johansson, T., Malmer, N., Jammet, M., Dengel, S., Kettner, E., Parmentier, F.-J. W., Wik, M.,](#)

Formatted: Indent: Left: 0 cm, First line: 0 cm

Formatted: Font: (Default) +Body (Calibri), Not Italic

Formatted: Font: (Default) +Body (Calibri)

Formatted: Font: (Default) +Body (Calibri), Not Italic

Formatted: Font: (Default) +Body (Calibri)

Formatted: Indent: Left: 0 cm, First line: 0 cm

Formatted: Font: (Default) +Body (Calibri), Not Italic

Formatted: Font: (Default) +Body (Calibri)

Formatted: Indent: Left: 0 cm, First line: 0 cm

Formatted: Font: (Default) +Body (Calibri), Not Italic

Formatted: Font: (Default) +Body (Calibri)

Formatted: Font: (Default) +Body (Calibri), Not Italic

Formatted: Font: (Default) +Body (Calibri)

Formatted: Indent: Left: 0 cm, First line: 0 cm

Formatted: Font: (Default) +Body (Calibri), Not Italic

Formatted: Font: (Default) +Body (Calibri)

Formatted: Font: (Default) +Body (Calibri), Not Italic

Formatted: Font: (Default) +Body (Calibri)

959 Crill, P. M., and Friborg, T., Åkerman, J.: Year-round CH₄ and CO₂ flux dynamics in two
 960 contrasting freshwater ecosystems of the subarctic, *14*, 5189–5216,
 961 <https://doi.org/10.5194/bg-14-5189-2017>, 2017.

962 JOHANSSON, T., MALMER, N., CRILL, P. M., FRIBORG, T., ÅKERMAN, J. H.,
 963 MastepanovMASTEPANOV, M., & Christensenand CHRISTENSEN, T. R.-(2006)-.: Decadal
 964 vegetation changes in a northern peatland, greenhouse gas fluxes and net radiative forcing-
 965 *Global Change Biology*, *Glob. Chang. Biol.*, *12*(12), 2352–2369.
 966 <https://doi.org/10.1111/j.1365-2486.2006.01267.x>, 2006.

967 Kirschke, S., Bousquet, P., Ciais, P., Saunio, M., Canadell, J. G., Dlugokencky, E. J.,
 968 Bergamaschi, P., Bergmann, D., Blake, D. R., Bruhwiler, L., Cameron-Smith, P., Castaldi, S.,
 969 Chevallier, F., Feng, L., Fraser, A., Heimann, M., Hodson, E. L., Houweling, S., Josse, B., Fraser, P.
 970 J., Krummel, P. B., Lamarque, J.-F., Langenfelds, R. L., Le Quéré, C., Naik, V., O’Doherty, S.,
 971 Palmer, P. I., Pison, I., Plummer, D., Poulter, B., Prinn, R. G., Rigby, M., Ringeval, B., Santini, M.,
 972 Schmidt, M., Shindell, D. T., Simpson, I. J., Spahni, R., Steele, L. P., Strode, S. A., Sudo, K., Szopa,
 973 S., van der Werf, G. R., Voulgarakis, A., van Weele, M., Weiss, R. F., Williams, J. E., and Zeng, G-
 974 (2013)-.: Three decades of global methane sources and sinks-*Nature Geoscience*, *Nat. Geosci.*,
 975 *6*(10), 813–823. <https://doi.org/10.1038/ngeo1955>, 2013.

976 Kljun, N., Calanca, P., Rotach, M. W., & Schmid, H. P.-(2015)-.: A simple two-dimensional
 977 parameterisation for Flux Footprint Prediction (FFP)-, *Geosci. Model Dev.*, *8*(11), 3695–3713.
 978 <https://doi.org/10.5194/gmd-8-3695-2015>, 2015.

979 Knox, S. H., Matthes, J. H., Sturtevant, C., Oikawa, P. Y., Verfaillie, J., & Baldocchi, D-
 980 (2016)-.: Biophysical controls on interannual variability in ecosystem-scale CO₂ and CH₄
 981 exchange in a California rice paddy-*Journal of Geophysical Research*, *J. Geophys. Res.*,
 982 *Biogeosciences*, *121*(3), 978–1001. <https://doi.org/10.1002/2015JG003247>, 2016.

983 Knox, S. H., Windham-Myers, L., Anderson, F., Sturtevant, C., and Bergamaschi, B.: Direct and
 984 Indirect Effects of Tides on Ecosystem-Scale CO₂ Exchange in a Brackish Tidal Marsh in Northern
 985 California, *J. Geophys. Res. Biogeosciences*, *123*, 787–806,
 986 <https://doi.org/10.1002/2017JG004048>, 2018.

987 Kowalska, N., Chojnicki, B., Rinne, J., Haapanala, S., Siedlecki, P., Urbaniak, M., Juszcak, R.,
 988 and Olejnik, J.-(2013)-.: Measurements of methane emission from a temperate wetland by eddy
 989 covariance method-*International, Int. Agrophysics*, *27*, 283–290.
 990 <https://doi.org/10.2478/v10247-012-0096-5>, 2013.

991 Levenberg, K. (1944). A method for the solution of certain non-linear problems in least squares-
 992 *Quarterly of Applied Mathematics*, *2*(2), 164–168. Retrieved from
 993 <http://www.jstor.org/stable/43633451>

994 LEVENBERG, K.: A METHOD FOR THE SOLUTION OF CERTAIN NON-LINEAR PROBLEMS IN LEAST
 995 SQUARES, *Q. Appl. Math.*, *2*, 164–168, 1944.

996 Li, T., Raivonen, M., Alekseychik, P., Aurela, M., Lohila, A., Zheng, X., Zhang, Q., Wang, G.,
 997 Mammarella, I., Rinne, J., Yu, L., Xie, B., Vesala, T., and Zhang, W.-(2016)-.: Importance of

Formatted: Indent: Left: 0 cm, First line: 0 cm

Formatted: Font: (Default) +Body (Calibri), Not Italic

Formatted: Font: (Default) +Body (Calibri)

Formatted: Font: (Default) +Body (Calibri), Not Italic

Formatted: Font: (Default) +Body (Calibri)

Formatted: Font: (Default) +Body (Calibri), Not Italic

Formatted: Font: (Default) +Body (Calibri)

Formatted: Font: (Default) +Body (Calibri), Not Italic

Formatted: Font: (Default) +Body (Calibri)

Formatted: Font: (Default) +Body (Calibri), Not Italic

Formatted: Font: (Default) +Body (Calibri)

Formatted: Font: (Default) +Body (Calibri), Not Italic

Formatted: Font: (Default) +Body (Calibri)

Formatted: Indent: Left: 0 cm, First line: 0 cm

Formatted: Font: (Default) +Body (Calibri), Not Italic

Formatted: Font: (Default) +Body (Calibri)

Formatted: Font: (Default) +Body (Calibri), Not Italic

Formatted: Font: (Default) +Body (Calibri)

Formatted: Font: (Default) +Body (Calibri), English (United States)

Formatted: Indent: Left: 0 cm, First line: 0 cm

Formatted: Font: (Default) +Body (Calibri)

Formatted: Font: (Default) +Body (Calibri), English (United States)

Formatted: Font: (Default) +Body (Calibri)

998 vegetation classes in modeling CH4 emissions from boreal and subarctic wetlands in Finland-
999 *Science of The, Sci. Total Environ., Environ.*, 572, 1111–1122-
1000 <https://doi.org/https://doi.org/10.1016/j.scitotenv.2016.08.020>, 2016.

1001 LUNDEGÅRDH, H.: CARBON DIOXIDE EVOLUTION OF SOIL AND CROP GROWTH, *Soil Sci.*, 23,
1002 1927.

1003 Malmer, N., Johansson, T., Olsrud, M., & Christensen, T. R. (2005).: Vegetation, climatic
1004 changes and net carbon sequestration in a North-Scandinavian subarctic mire over 30 years-
1005 *Global Change Biology, Glob. Chang. Biol.*, 11(11), 1895–1909-
1006 <https://doi.org/10.1111/j.1365-2486.2005.01042.x>, 2005.

1007 Marquardt, D. W. (1963).: An Algorithm for Least-Squares Estimation of Nonlinear Parameters-
1008 *Journal of the Society for Industrial and Applied Mathematics, J. Soc. Ind. Appl. Math.*, 11(2),
1009 431–441. Retrieved from <http://www.jstor.org/stable/2098941>, 1963.

1010 Mastepanov, M., Sigsgaard, C., Dlugokencky, E. J., Houweling, S., Ström, L., Tamstorf, M. P., and
1011 Christensen, T. R.: Large tundra methane burst during onset of freezing, *Nature*, 456, 628–630,
1012 <https://doi.org/10.1038/nature07464>, 2008.

1013 Mastepanov, M., Sigsgaard, C., Tagesson, T., Ström, L., Tamstorf, M. P., Lund, M., &
1014 Christensen, T. R. (2013).: Revisiting factors controlling methane emissions from high-Arctic
1015 tundra. *Biogeosciences*, 10(7), 5139–5158. <https://doi.org/10.5194/bg-10-5139-2013>.

1016 Mastepanov, Mikhail, Sigsgaard, C., Dlugokencky, E. J., Houweling, S., Ström, L., Tamstorf, M. P.,
1017 & Christensen, T. R. (2008). Large tundra methane burst during onset of freezing. *Nature*,
1018 456(7222), 628–630. <https://doi.org/10.1038/nature07464>

1019 Mauder, M., & Foken, T. (2011).: Documentation and Instruction Manual of the Eddy
1020 Covariance Software Package TK2. Arbeitsergebnisse, *Universität Univ.* Bayreuth, Abteilung
1021 Mikrometeorologie, ISSN 1614-8916, 46. <https://doi.org/10.5194/bg-5-451-2008>, 2011.

1022 McCalley, C. K., Woodcroft, B. J., Hodgkins, S. B., Wehr, R. A., Kim, E.-H., Mondav, R., Crill, P.
1023 M., Chanton, J. P., Rich, V. I., Tyson, G. W., and Saleska, S. R. (2014).: Methane dynamics
1024 regulated by microbial community response to permafrost thaw. *Nature*, 514(7523), 478–
1025 481. <https://doi.org/10.1038/nature13798>, 2014.

1026 McGuire, A. D., Christensen, T. R., Hayes, D., Heroult, A., Euskirchen, E., Kimball, J. S., Koven, C.,
1027 Lafleur, P., Miller, P. A., Oechel, W., Peylin, P., Williams, M., and Yi, Y.: An assessment of the
1028 carbon balance of Arctic tundra: comparisons among observations, process models, and
1029 atmospheric inversions, 9, 3185–3204, <https://doi.org/10.5194/bg-9-3185-2012>, 2012.

1030 Melloh, R. A. and Crill, P. M.: Winter methane dynamics in a temperate peatland, *Global*
1031 *Biogeochem. Cycles*, 10, 247–254, <https://doi.org/doi:10.1029/96GB00365>, 1996.

1032 Mikhaylov, O. A., Miglovets, M. N., & Zagirova, S. V. (2015).: Vertical methane fluxes in
1033 mesooligotrophic boreal peatland in European Northeast Russia. *Contemporary Problems of*
1034 *Ecology, Contemp. Probl. Ecol.*, 8(3), 368–375. <https://doi.org/10.1134/S1995425515030099>,
1035 2015.

Formatted

Formatted: Indent: Left: 0 cm, First line: 0 cm

Formatted

Formatted

Formatted

Formatted: Indent: Left: 0 cm, First line: 0 cm

Formatted

Formatted: Indent: Left: 0 cm, First line: 0 cm

Formatted

Formatted

Formatted: Font: (Default) +Body (Calibri)

Formatted: Font: (Default) +Body (Calibri), English (United States)

Formatted: Indent: Left: 0 cm, First line: 0 cm

Formatted

1036 [Moorcroft, P., Wofsy, S., Dunn, A., and Ise, T.: High sensitivity of peat decomposition to climate](#)
1037 [change through water-table feedback, Nat. Geosci., 1, <https://doi.org/10.1038/ngeo331>, 2008.](#)

1038 [Natali, S. M., Watts, J. D., Rogers, B. M., Potter, S., Ludwig, S. M., Selbmann, A.-K., Sullivan, P. F.,](#)
1039 [Abbott, B. W., Arndt, K. A., Birch, L., Björkman, M. P., Bloom, A. A., Celis, G., Christensen, T. R.,](#)
1040 [Christiansen, C. T., Commane, R., Cooper, E. J., Crill, P., Czimczik, C., Davydov, S., Du, J., Egan, J.](#)
1041 [E., Elberling, B., Euskirchen, E. S., Friborg, T., Genet, H., Göckede, M., Goodrich, J. P., Grogan, P.,](#)
1042 [Helbig, M., Jafarov, E. E., Jastrow, J. D., Kalhori, A. A. M., Kim, Y., Kimball, J. S., Kutzbach, L.,](#)
1043 [Lara, M. J., Larsen, K. S., Lee, B.-Y., Liu, Z., Lorant, M. M., Lund, M., Lupascu, M., Madani, N.,](#)
1044 [Malhotra, A., Matamala, R., McFarland, J., McGuire, A. D., Michelsen, A., Minions, C., Oechel,](#)
1045 [W. C., Olefeldt, D., Parmentier, F.-J. W., Pirk, N., Poulter, B., Quinton, W., Rezanezhad, F., Risk,](#)
1046 [D., Sachs, T., Schaefer, K., Schmidt, N. M., Schuur, E. A. G., Semenchuk, P. R., Shaver, G.,](#)
1047 [Sonnentag, O., Starr, G., Treat, C. C., Waldrop, M. P., Wang, Y., Welker, J., Wille, C., Xu, X.,](#)
1048 [Zhang, Z., Zhuang, Q., and Zona, D.: Large loss of CO₂ in winter observed across the northern](#)
1049 [permafrost region, Nat. Clim. Chang., 9, 852–857, <https://doi.org/10.1038/s41558-019-0592-8>,](#)
1050 [2019.](#)

1051 [Nemitz, E., Mammarella, I., Ibrom, A., Aurela, M., Burba, G., Dengel, S., Gielen, B., Grelle, A.,](#)
1052 [Heinesch, B., Herbst, M., Hörtnagl, L., Klemetsson, L., Lindroth, A., Lohila, A., Mcdermitt, D.,](#)
1053 [Meier, P., Merbold, L., Nelson, D., Nicolini, G., and Zahniser, M.: Standardisation of eddy-](#)
1054 [covariance flux measurements of methane and nitrous oxide, Int. Agrophysics, 32, 517–549,](#)
1055 [https://doi.org/10.1515/intag-2017-0042, 2018.](#)

1056 NILSSON, M., SAGERFORS, J., BUFFAM, I., LAUDON, H., ERIKSSON, T., GRELE, A.,
1057 ~~---~~[KLEMETSSON, L., WESLIEN, P. E. R., and LINDROTH, A. \(2008\).](#): Contemporary carbon
1058 accumulation in a boreal oligotrophic minerogenic mire – a significant sink after accounting for
1059 all C-fluxes. ~~Global Change Biology, Glob. Chang. Biol., 14(10), 2317–2332.~~
1060 <https://doi.org/10.1111/j.1365-2486.2008.01654.x>, 2008.

1061 [Nisbet, E. G., Dlugokencky, E. J., and Bousquet, P.: Methane on the Rise—Again, Science \(80-](#)
1062 [\), 343, 493 LP – 495, <https://doi.org/10.1126/science.1247828>, 2014.](#)

1063 [Nisbet, E. G., Dlugokencky, E. J., Manning, M. R., Lowry, D., Fisher, R. E., France, J. L., ~~---~~Michel,](#)
1064 [S. E., Miller, J. B., White, J. W. C., Vaughn, B., Bousquet, P., Pyle, J. A., Warwick, N. J., Cain, M.,](#)
1065 [Brownlow, R., Zazzeri, G., Lanoisellé, M., Manning, A. C., Gloor, E., Worthy, D. E. J., Brunke, E.-](#)
1066 [G., Labuschagne, C., Wolff, E. W., and Ganesan, A. L. \(2016\).](#): Rising atmospheric methane:
1067 2007–2014 growth and isotopic shift. ~~Global Biogeochemical Cycles, 30(9), 1356–~~
1068 [1370.](https://doi.org/10.1002/2016GB005406) <https://doi.org/10.1002/2016GB005406>, 2016.

1069 [Nisbet, Euan G., Dlugokencky, E. J., & Bousquet, P. \(2014\).of Sciences Engineering and Medicine:](#)
1070 [Improving Characterization of Anthropogenic Methane onEmissions in the Rise—Again. Science,](#)
1071 [343\(6170\), 493 LP – 495,United States, The National Academies Press, Washington, DC,](#)
1072 <https://doi.org/10.1126/science.124782817226/24987>, 2018.

1073 [Olefeldt, D., Roulet, N. T., Bergeron, O., Crill, P., Bäckstrand, K., and Christensen, T. R.: Net](#)
1074 [carbon accumulation of a high-latitude permafrost palsa mire similar to permafrost-free](#)
1075 [peatlands, Geophys. Res. Lett., 39, <https://doi.org/10.1029/2011GL050355>, 2012.](#)

Formatted: Indent: Left: 0 cm, First line: 0 cm

Formatted: Font: (Default) +Body (Calibri), Not Italic

Formatted: Font: (Default) +Body (Calibri)

Formatted: Indent: Left: 0 cm, First line: 0 cm

Formatted: Font: (Default) +Body (Calibri), Not Italic

Formatted: Font: (Default) +Body (Calibri)

Formatted: Font: (Default) +Body (Calibri), Not Italic

Formatted: Font: (Default) +Body (Calibri)

Formatted: Font: (Default) +Body (Calibri), Not Italic

Formatted: Font: (Default) +Body (Calibri)

Formatted: Font: (Default) +Body (Calibri), English (United States)

Formatted: Font: (Default) +Body (Calibri)

1076 [Parmentier, F. J. W., van Huissteden, J., van der Molen, M. K., Schaepman-Strub, G., Karsanaev,](#)
1077 [S. A., Maximov, T. C., and Dolman, A. J.: Spatial and temporal dynamics in eddy covariance](#)
1078 [observations of methane fluxes at a tundra site in northeastern Siberia, *J. Geophys. Res.*](#)
1079 [Biogeosciences, 116, <https://doi.org/10.1029/2010JG001637>, 2011.](#)

1080 [Post, E., Alley, R. B., Christensen, T. R., Macias-Fauria, M., Forbes, B. C., Gooseff, M. N., ~~Miller, A.,~~](#)
1081 [Kerby, J. T., Laidre, K. L., Mann, M. E., Olofsson, J., Stroeve, J. C., Ulmer, F., Virginia, R. A., and](#)
1082 [Wang, M. \(2019\).: The polar regions in a 2{\[textdegree\]}C warmer world. *Science Advances, Sci.*](#)
1083 [Adv., 5\(12\). <https://doi.org/10.1126/sciadv.aaw9883>, 2019.](#)

1084 [Pugh, C. A., Reed, D. E., Desai, A. R., ~~&and~~ Sulman, B. N. \(2018\).: Wetland flux controls: how](#)
1085 [does interacting water table levels and temperature influence carbon dioxide and methane](#)
1086 [fluxes in northern Wisconsin? *Biogeochemistry*, 137\(1\), 15–25.](#)
1087 [<https://doi.org/10.1007/s10533-017-0414-x>, 2018.](#)

1088 [Raz-Yaseef, N., Torn, M. S., Wu, Y., Billesbach, D. P., Liljedahl, A. K., Kneafsey, T. J., ~~---~~](#)
1089 [Romanovsky, V. E., Cook, D. R., and Wulschleger, S. D. \(2017\).: Large CO₂ and CH₄ emissions](#)
1090 [from polygonal tundra during spring thaw in northern Alaska. *Geophysical Research Letters,*](#)
1091 [*Geophys. Res. Lett.*, 44\(1\), 504–513. <https://doi.org/10.1002/2016GL071220>, 2017.](#)

1092 [Rebmann, C., Aubinet, M., Schmid, H., Arriga, N., Aurela, M., Burba, G., ~~---~~ Clement, R., De Ligne,](#)
1093 [A., Fratini, G., Gielen, B., Grace, J., Graf, A., Gross, P., Haapanala, S., Herbst, M., Hörtnagl, L.,](#)
1094 [Ibrom, A., Joly, L., Kljun, N., and Franz, D. \(2018\).: ICOS eddy covariance flux-station site setup:](#)
1095 [A review. *International, Int. Agrophysics*, 32, 471–494. \[0044, 2018.\]\(https://doi.org/10.1515/intag-2017-</u>
1096 <u><a href=\)](#)

1097 [Rinne, J., Tuovinen, J.-P., Klemedtsson, L., Aurela, M., Holst, J., Lohila, A., ... Nilsson, M. B. \(2020\).](#)
1098 [Effect of the 2018 European drought on methane and carbon dioxide exchange of](#)
1099 [northern mire ecosystems. *Philosophical Transactions of the Royal Society B: Biological*](#)
1100 [*Sciences*, 375\(1810\), 20190517. <https://doi.org/10.1098/rstb.2019.0517>](#)

1101 [Rinne, Janne, Rindskopf, D.: Generalized linear models., <https://doi.org/10.1037/13621-009>,](#)
1102 [2012.](#)

1103 [Rinne, J., Riutta, T., Pihlatie, M., Aurela, M., Haapanala, S., Tuovinen, J.-P., ~~---~~ Tuittila, E.-S., and](#)
1104 [Vesala, T. \(2007\).: Annual cycle of methane emission from a boreal fen measured by the eddy](#)
1105 [covariance technique. *Tellus B: Chemical and Physical Meteorology, Chem. Phys. Meteorol.*,](#)
1106 [59\(3\), 449–457. <https://doi.org/10.1111/j.1600-0889.2007.00261.x>, 2007.](#)

1107 [Rinne, Janne, J., Tuittila, E.-S., Peltola, O., Li, X., Raivonen, M., Alekseychik, P., ~~---~~ Haapanala, S.,](#)
1108 [Pihlatie, M., Aurela, M., Mammarella, I., and Vesala, T. \(2018\).: Temporal Variation of](#)
1109 [Ecosystem Scale Methane Emission From a Boreal Fen in Relation to Temperature, Water Table](#)
1110 [Position, and Carbon Dioxide Fluxes. *Global Biogeochemical Biogeochem. Cycles*, 32\(7\), 1087–](#)
1111 [1106. <https://doi.org/10.1029/2017GB005747>, 2018.](#)

1112 [Saunio, M., Stavert, A. R., Poulter, B., Bousquet, P., Canadell, J. G., Jackson, R. B., ... Zhuang, Q.](#)
1113 [\(2020\). The Global Methane Budget 2000–2017. *Earth System Science Data*, 12\(3\), 1561–](#)
1114 [1623. <https://doi.org/10.5194/essd-12-1561-2020>](#)

Formatted	...
Formatted	...
Formatted	...
Formatted	...
Formatted	...
Formatted	...
Formatted	...
Formatted	...
Formatted	...
Formatted	...
Formatted	...
Formatted	...
Formatted	...
Formatted	...
Formatted	...
Formatted	...
Formatted	...
Formatted	...
Formatted	...
Formatted	...
Formatted	...
Formatted	...
Formatted	...
Formatted	...
Formatted	...
Formatted	...
Formatted	...
Formatted	...
Formatted	...
Formatted	...
Formatted	...
Formatted	...
Formatted	...
Formatted	...
Formatted	...
Formatted	...

1115 [Rinne, J., Tuovinen, J.-P., Klemedtsson, L., Aurela, M., Holst, J., Lohila, A., Weslien, P., Vestin, P.,](#)
1116 [Łakomiec, P., Peichl, M., Tuittila, E.-S., Heiskanen, L., Laurila, T., Li, X., Alekseychik, P.,](#)
1117 [Mammarella, I., Ström, L., Crill, P., and Nilsson, M. B.: Effect of the 2018 European drought on](#)
1118 [methane and carbon dioxide exchange of northern mire ecosystems, *Philos. Trans. R. Soc. B*](#)
1119 [Biol. Sci., 375, 20190517, <https://doi.org/10.1098/rstb.2019.0517>, 2020.](#)

1120 [Robertson, A. M., Edie, R., Snare, D., Soltis, J., Field, R. A., Burkhart, M. D., Bell, C. S., Zimmerle,](#)
1121 [D., and Murphy, S. M.: Variation in Methane Emission Rates from Well Pads in Four Oil and Gas](#)
1122 [Basins with Contrasting Production Volumes and Compositions, *Environ. Sci. Technol.*, 51,](#)
1123 [8832–8840, <https://doi.org/10.1021/acs.est.7b00571>, 2017.](#)

1124 [Röckmann, T., Eyer, S., Veen, C., Popa, E., Tuzson, B., Monteil, G., Houweling, S., Harris, E.,](#)
1125 [Brunner, D., Fischer, H., Zazzeri, G., Lowry, D., Nisbet, E., Brand, W., Necki, J., Emmenegger, L.,](#)
1126 [and Mohn, J.: In situ observations of the isotopic composition of methane at the Cabauw tall](#)
1127 [tower site, *Atmos. Chem. Phys.*, 16, 10469–10487, <https://doi.org/10.5194/acp-16-10469-2016>,](#)
1128 [2016.](#)

1129 [Rößger, N., Wille, C., Holl, D., Göckede, M., and Kutzbach, L.: Scaling and balancing carbon](#)
1130 [dioxide fluxes in a heterogeneous tundra ecosystem of the Lena River Delta, 16, 2591–2615,](#)
1131 [https://doi.org/10.5194/bg-16-2591-2019, 2019.](#)

1132 [Saunio, M., Bousquet, P., Poulter, B., Peregón, A., Ciais, P., Canadell, J. G., Dlugokencky, E. J.,](#)
1133 [Etiopio, G., Bastviken, D., Houweling, S., Janssens-Maenhout, G., Tubiello, F. N., Castaldi, S.,](#)
1134 [Jackson, R. B., Alexe, M., Arora, V. K., Beerling, D. J., Bergamaschi, P., Blake, D. R., Brailsford, G.,](#)
1135 [Brovkin, V., Bruhwiler, L., Crevoisier, C., Crill, P., Covey, K., Curry, C., Frankenberg, C., Gedney,](#)
1136 [N., Höglund-Isaksson, L., Ishizawa, M., Ito, A., Joos, F., Kim, H.-S., Kleinen, T., Krummel, P.,](#)
1137 [Lamarque, J.-F., Langenfelds, R., Locatelli, R., Machida, T., Maksyutov, S., McDonald, K. C.,](#)
1138 [Marshall, J., Melton, J. R., Morino, I., Naik, V., O'Doherty, S., Parmentier, F.-J. W., Patra, P. K.,](#)
1139 [Peng, C., Peng, S., Peters, G. P., Pison, I., Prigent, C., Prinn, R., Ramonet, M., Riley, W. J., Saito,](#)
1140 [M., Santini, M., Schroeder, R., Simpson, I. J., Spahni, R., Steele, P., Takizawa, A., Thornton, B. F.,](#)
1141 [Tian, H., Tohjima, Y., Viovy, N., Voulgarakis, A., van Weele, M., van der Werf, G. R., Weiss, R.,](#)
1142 [Wiedinmyer, C., Wilton, D. J., Wiltshire, A., Worthy, D., Wunch, D., Xu, X., Yoshida, Y., Zhang, B.,](#)
1143 [Zhang, Z., and Zhu, Q.: The global methane budget 2000–2012, *Earth Syst. Sci. Data*, 8, 697–](#)
1144 [751, <https://doi.org/10.5194/essd-8-697-2016>, 2016.](#)

1145 [Saunio, M., Stavert, A. R., Poulter, B., Bousquet, P., Canadell, J. G., Jackson, R. B., Raymond, P.](#)
1146 [A., Dlugokencky, E. J., Houweling, S., Patra, P. K., Ciais, P., Arora, V. K., Bastviken, D.,](#)
1147 [Bergamaschi, P., Blake, D. R., Brailsford, G., Bruhwiler, L., Carlson, K. M., Carrol, M., Castaldi, S.,](#)
1148 [Chandra, N., Crevoisier, C., Crill, P. M., Covey, K., Curry, C. L., Etiopio, G., Frankenberg, C.,](#)
1149 [Gedney, N., Hegglin, M. I., Höglund-Isaksson, L., Hugelius, G., Ishizawa, M., Ito, A., Janssens-](#)
1150 [Maenhout, G., Jensen, K. M., Joos, F., Kleinen, T., Krummel, P. B., Langenfelds, R. L., Laruelle, G.](#)
1151 [G., Liu, L., Machida, T., Maksyutov, S., McDonald, K. C., McNorton, J., Miller, P. A., Melton, J. R.,](#)
1152 [Morino, I., Müller, J., Murguía-Flores, F., Naik, V., Niwa, Y., Noce, S., O'Doherty, S., Parker, R. J.,](#)
1153 [Peng, C., Peng, S., Peters, G. P., Prigent, C., Prinn, R., Ramonet, M., Regnier, P., Riley, W. J.,](#)
1154 [Rosentreter, J. A., Segers, A., Simpson, I. J., Shi, H., Smith, S. J., Steele, L. P., Thornton, B. F.,](#)
1155 [Tian, H., Tohjima, Y., Tubiello, F. N., Tsuruta, A., Viovy, N., Voulgarakis, A., Weber, T. S., van](#)

1156 [Weele, M., van der Werf, G. R., Weiss, R. F., Worthy, D., Wunch, D., Yin, Y., Yoshida, Y., Zhang,](#)
1157 [W., Zhang, Z., Zhao, Y., Zheng, B., Zhu, Q., Zhu, Q., and Zhuang, Q.: The Global Methane Budget](#)
1158 [2000--2017, Earth Syst. Sci. Data, 12, 1561–1623, <https://doi.org/10.5194/essd-12-1561-2020>,](#)
1159 [2020.](#)

1160 [Song, C., Xu, X., Sun, X., Tian, H., Sun, L., Miao, Y., ~~Wang, X., and Guo, Y. \(2012\).~~](#) Large
1161 methane emission upon spring thaw from natural wetlands in the northern permafrost region-
1162 [Environmental Research Letters, Environ. Res. Lett., 7\(3\), 034009,](#)
1163 <https://doi.org/10.1088/1748-9326/7/3/034009>, 2012.

1164 [Sturtevant, C. S., Oechel, W. C., Zona, D., Kim, Y., & Emerson, C. E. \(2012\).](#) Soil moisture
1165 control over autumn season methane flux, Arctic Coastal Plain of Alaska-[Biogeosciences, 9\(4\),](#)
1166 [1423–1440,](#) <https://doi.org/10.5194/bg-9-1423-2012>, 2012.

1167 [T, V., Eugster, W., and Ojala, A.: Eddy Covariance: A Practical Guide to Measurement and Data](#)
1168 [Analysis, in: Springer Atmospheric Sciences Series, vol. 12, 365–376,](#)
1169 <https://doi.org/10.1007/978-94-007-2351-1>, 2012.

1170 [Taylor, M. A., Celis, G., Ledman, J. D., Bracho, R., & Schuur, E. A. G. \(2018\).](#) Methane Efflux
1171 Measured by Eddy Covariance in Alaskan Upland Tundra Undergoing Permafrost Degradation-
1172 [Journal of Geophysical Research, J. Geophys. Res., Biogeosciences, 123\(9\),](#)
1173 <https://doi.org/10.1029/2018JG004444>, 2018.

1174 [Turetsky, M. R., Kotowska, A., Bubier, J., Dise, N. B., Crill, P., Hornibrook, E. R. C., ~~Minkinen,~~](#)
1175 [K., Moore, T. R., Myers-Smith, I. H., Nykänen, H., Olefeldt, D., Rinne, J., Saarnio, S., Shurpali, N.,](#)
1176 [Tuittila, E.-S., Waddington, J. M., White, J. R., Wickland, K. P., and Wilkening, M. \(2014\).](#) A
1177 synthesis of methane emissions from 71 northern, temperate, and subtropical wetlands-[Global](#)
1178 [Change Biology, Glob. Chang. Biol., 20\(7\),](#) 2183–2197. <https://doi.org/10.1111/gcb.12580>,
1179 [2014.](#)

1180 [Vellinga, O. S., Dobosy, R. J., Dumas, E. J., Gioli, B., Elbers, J. A., and Hutjes, R. W. A.: Calibration](#)
1181 [and Quality Assurance of Flux Observations from a Small Research Aircraft*, J. Atmos. Ocean.](#)
1182 [Technol., 30, 161–181, <https://doi.org/10.1175/JTECH-D-11-00138.1>, 2013.](#)

1183 [Verma, S. B., Baldocchi, D. D., Anderson, D. E., Matt, D. R., & Clement, R. J. \(1986\).](#) Eddy
1184 fluxes of CO₂, water vapor, and sensible heat over a deciduous forest-[Boundary-Layer](#)
1185 [Meteorology, Meteorol., 36\(1\),](#) 71–91. <https://doi.org/10.1007/BF00117459>, 1986.

1186 [Woodcroft, B. J., Singleton, C. M., Boyd, J. A., Evans, P. N., Emerson, J. B., Zayed, A. A. F.,](#)
1187 [Hoelzle, R. D., Lamberton, T. O., McCalley, C. K., Hodgkins, S. B., Wilson, R. M., Purvine, S. O.,](#)
1188 [Nicora, C. D., Li, C., Frohling, S., Chanton, J. P., Crill, P. M., Saleska, S. R., Rich, V. I., and Tyson, G.](#)
1189 [W.: Genome-centric view of carbon processing in thawing permafrost, Nature, 560, 49–54,](#)
1190 <https://doi.org/10.1038/s41586-018-0338-1>, 2018.

1191 [Wutzler, T., Lucas-Moffat, A., Migliavacca, M., Knauer, J., Sickel, K., Šigut, L., ~~Menzer, O., and~~](#)
1192 [Reichstein, M. \(2018\).](#) Basic and extensible post-processing of eddy covariance flux data with
1193 REddyProc-[Biogeosciences, 15\(16\),](#) 5015–5030. <https://doi.org/10.5194/bg-15-5015-2018>,
1194 [2018.](#)

Formatted: Font: (Default) +Body (Calibri), English (United States)

Formatted: Font: (Default) +Body (Calibri), English (United States)

Formatted: Indent: Left: 0 cm, First line: 0 cm

Formatted: Font: (Default) +Body (Calibri)

Formatted: Font: (Default) +Body (Calibri)

Formatted: Font: (Default) +Body (Calibri), Not Italic

Formatted: Font: (Default) +Body (Calibri)

Formatted: Font: (Default) +Body (Calibri), Not Italic

Formatted: Font: (Default) +Body (Calibri)

Formatted: Indent: Left: 0 cm, First line: 0 cm

Formatted: Font: (Default) +Body (Calibri), Not Italic

Formatted: Font: (Default) +Body (Calibri)

Formatted: Font: (Default) +Body (Calibri), Not Italic

Formatted: Font: (Default) +Body (Calibri)

Formatted: Font: (Default) +Body (Calibri), Not Italic

Formatted: Font: (Default) +Body (Calibri)

Formatted: Indent: Left: 0 cm, First line: 0 cm

Formatted: Font: (Default) +Body (Calibri), Not Italic

Formatted: Font: (Default) +Body (Calibri)

Formatted: Font: (Default) +Body (Calibri), Not Italic

Formatted: Font: (Default) +Body (Calibri)

Formatted: Indent: Left: 0 cm, First line: 0 cm

Formatted: Font: (Default) +Body (Calibri), Not Italic

Formatted: Font: (Default) +Body (Calibri)

1195 Yamulki, S., Anderson, R., Peace, A., ~~&and~~ Morison, J. I. L. ~~(2013)~~.: Soil ~~CO₂-CH₄CO₂~~ ~~{2}~~
1196 ~~CH₄~~ ~~{4}~~ and ~~N₂O~~ ~~{2}~~ ~~SO~~ fluxes from an afforested lowland raised peatbog in Scotland:
1197 implications for drainage and restoration. ~~*Biogeosciences*, 10(2), 1051–1065.~~
1198 <https://doi.org/10.5194/bg-10-1051-2013>, 2013.

1199 ~~Zhang, Z., Zimmermann, N. E., Stenke, A., Li, X., Hodson, E. L., Zhu, G., Huang, C., and Poulter,~~
1200 ~~B.: Emerging role of wetland methane emissions in driving 21st century climate change, Proc.~~
1201 ~~Natl. Acad. Sci., 114, 9647–9652, <https://doi.org/10.1073/pnas.1618765114>, 2017.~~

1202 ~~Zhang, Z., Zimmermann, N. E., Stenke, A., Li, X., Hodson, E. L., Zhu, G., ... Poulter, B. (2017).~~
1203 ~~Emerging role of wetland methane emissions in driving 21st century climate change.~~
1204 ~~*Proceedings of the National Academy of Sciences*, 114(36), 9647–9652.~~
1205 ~~<https://doi.org/10.1073/pnas.1618765114>~~

1206

Formatted: Font: (Default) +Body (Calibri), Not Italic

Formatted: Font: (Default) +Body (Calibri)

Formatted: Font: (Default) +Body (Calibri)

Field Code Changed

Formatted: Left, Line spacing: single, No widow/orphan control, Don't adjust space between Latin and Asian text, Don't adjust space between Asian text and numbers